

Transport of groundwater contaminant through high density ATEs regions

The effects of well placement on spreading and dilution

Host organization: KWR Water Research Institute

Groningehaven 7

3433 PE, Nieuwegein

Supervisors: Prof. Dr. Ruud Schotting (UU)

Dr. Niels Hartog (KWR & UU)

Dr. Ir. Martin Bloemendal (KWR & TU Delft)

Date: 21-2-2021

Author: M.M.A. Ketelaars

4290860



Universiteit Utrecht

KWR

Abstract

Aquifer Thermal Energy Storage (ATES) systems are a renewable energy technology which provides sustainable heating and cooling for the built environment. These systems store the surplus of thermal energy in summer and the deficit of thermal energy in winter in the groundwater to be able to recover this energy in the opposite season. The demand for ATES systems in cities is large, while aquifers beneath cities are often polluted. Therefore, the transport of contaminants through high density ATES regions is studied in this thesis.

The numerical SEAWAT model from the work of Jaxa-Rozen et al. (2015) was used. This model is created to study the temperature in the subsurface. To make the model suitable for studying contaminant spreading and dilution by ATES wells, a tracer contaminant was added as a second species and a method to model internal ATES transport was developed. First, the interaction between two doublets was studied for line and checkerboard patterns. In these 2x2 configurations, the distance between the wells, the well discharge and the ambient groundwater flow were systematically changed. Secondly, the spreading and dilution through an ATES region was studied with 4x4 well configurations.

The results showed that the spreading and dilution by the implementation of ATES systems increases drastically. The policy distances in the Netherlands now inhibit the negative interference of thermal performance, but do not inhibit the external ATES transport between systems. However, the impact can be managed/limited by choosing a suitable well configuration. This study showed that the external ATES transport between wells of the same type is dominated by dispersion, which causes small spreading rates in a timeframe of one year. The transport between two opposite type wells is governed by short circuit flow, which causes large spreading rates in a timeframe of one season. Therefore, line pattern doublets are preferred if spreading of contaminants needs to be limited. In practice, this means that it would be best if the same type of wells are clustered and the distance between the opposite wells is kept at least at the policy distance. This is also beneficial for the thermal efficiency of the wells.

The downside of placing wells in line pattern is that the hydraulic head differences become large, causing increased groundwater flow. This increased groundwater flow can cause increased leaching from constant contaminant sources into the groundwater. Further study needs to focus on expanding this knowledge on constant contaminant sources and the implementation of that knowledge in ATES planning.

Table of Contents

Table of Contents	2
1 Introduction	4
1.1 Influence of ATEs systems on contaminant spreading and dilution.....	4
1.2 Research goal.....	4
1.3 Approach and structure of report.....	5
2 Literature review	6
2.1 Working of ATEs systems.....	6
2.2 Thermal performance of an ATEs system	7
2.3 Thermal performance of multiple ATEs systems	7
2.4 ATEs induced spreading and dilution of contaminants.....	9
2.4.1 Well dilution	9
2.4.2 Dispersive dilution	9
2.4.3 Internal ATEs transport.....	10
2.4.4 Spreading by partial recovery	10
2.4.5 External ATEs transport.....	11
2.4.6 Increased leaching from contaminant sources due to increased groundwater flow.....	12
3 Methods and materials	13
3.1 Modeling software.....	13
3.1.1 MODFLOW.....	13
3.1.2 MT3DMS.....	13
3.1.3 SEAWAT	14
3.2 Model specifications	15
3.2.1 Model parameters	15
3.2.2 Model discretization	16
3.2.3 Modeled contaminant	18
3.2.4 Internal ATEs transport.....	18
3.3 Research approach	19
3.3.1 2x2 well configurations.....	20
3.3.1.1 Interaction between two doublets in line pattern.....	20
3.3.1.2 Interaction between two doublets in checkerboard pattern	21
3.3.2 Influence of ambient groundwater flow on the 2x2 well configurations.....	22
3.3.3 4x4 well configurations.....	22
3.4 Assessment criteria	23
3.4.1 Center of mass and variance	23
3.4.2 Plume area.....	24
3.4.3 Normalization	24
3.4.4 Output concentrations	25
4 Results.....	26

4.1	Interaction between two doublets in line pattern	26
4.1.1	Description of observed plume development	26
4.1.2	External ATES transport in line pattern.....	27
4.1.3	High and low density scenario	30
4.1.4	Conclusions.....	31
4.2	Interaction between two doublets in checkerboard pattern	32
4.2.1	Description observed plume development.....	32
4.2.2	External ATES transport in checkerboard pattern	33
4.2.3	High and low density scenario	34
4.2.4	Conclusions.....	35
4.3	Comparison of line and checkerboard pattern	36
4.4	Influence of ambient groundwater flow	37
4.4.1	Influence of ambient flow on the contaminant plume	37
4.4.2	Influence of different flow velocities on the contaminant plume.....	38
4.4.3	Conclusions.....	39
4.5	Interaction between 4x4 ATES regions and contaminants.....	40
4.5.1	Spreading and dilution in line and checkerboard regions.....	40
4.5.2	Conclusions.....	45
5	Discussion.....	46
5.1	Spreading and dilution by ATES systems.....	46
5.1.1	Spreading through ATES regions.....	46
5.1.2	Ambient flow	46
5.1.3	Partial recovery by well imbalance	47
5.1.4	Spreading and dilution by ATES systems with multiple wells.....	47
5.1.5	Increased leaching from a constant contaminant source.....	47
5.1.6	Management of contaminants	48
5.1.7	Implications for practice	48
5.2	Discussion on the used model	49
5.2.1	Internal ATES transport.....	49
5.2.2	Influence of initial contaminant.....	50
5.2.3	Extrapolation of 4x4 configurations to larger regions.....	50
5.3	Recommendations	51
6	Conclusion	52
	References	53
	List of symbols and units.....	55
	List of figures	56
	List of tables.....	58

1 Introduction

Aquifer Thermal Energy Storage (ATES) systems are a renewable energy technology. This technology uses the groundwater in aquifers to store and recover thermal energy in order to heat and cool buildings in a sustainable manner. The reason for application of ATES systems is the current unsustainable heat production combined with large heating demands. The estimated part of the energy consumption used for heating and cooling of buildings is 40 % in the Netherlands (Bloemendal and Hartog, 2018). Worldwide, 50% of the energy consumption is estimated to be used for heating and cooling (REN21, 2017).

Since the policy of the Netherlands, among other countries, is to reduce the greenhouse gas emissions, the popularity of the ATES systems increased. This increasing popularity cause high density ATES regions to emerge in the subsurface of cities. However, the shallow aquifers beneath cities utilized for ATES are often polluted (Zuurbier et al., 2013). Activities in the past where pollutants were spilled or discharged into the subsurface caused contaminant plumes and dense non-aqueous phase liquids (DNAPLs) to be present in the subsurface. The lack of regulations and administration of past events makes it difficult to map where and how much contamination is present. That is why ATES systems are placed in deeper aquifers if possible. However, in many countries and regions deeper aquifers are not present and the shallow aquifers are the only suitable location for ATES systems (Bloemendal et al., 2015), which are also used for many other functions like drinking water production. There is a lot of knowledge on hydrogeological transport phenomena, enabling hydrologists to predict the behavior of contaminants in relation to groundwater protection zones. However, when ATES systems are placed, enhanced spreading and dilution of contaminants becomes less predictable. This leads to the question what the impact, and the extent of the impact, of the placement of these systems is on the spreading of the contaminants present in aquifers utilized for ATES.

1.1 Influence of ATES systems on contaminant spreading and dilution

ATES systems influence the spreading and dilution of contaminants in multiple ways. Firstly, it causes enhanced head-driven flow due to pump activity. This increase in advection causes an increase in contaminant spreading. Secondly, vertical mixing occurs due to pumping and (re-)injecting of groundwater with fully penetrating wells. Thirdly, internal ATES transport takes place by extracting contaminant mass and injecting it on another location. And lastly the transfer of contaminants from one to neighboring ATES systems in the subsurface (Phernambucq, 2015). These mechanisms causing spreading and dilution are known. However, methods to assess and manage the influence of ATES systems on the spreading of the contaminants are lacking. This can lead to unforeseen enhanced spreading of contaminants. Or on the other hand, limit ATES adoption.

1.2 Research goal

Since the motivation for ATES application is providing sustainable heating, most studies are focused on optimizing thermal performance in order to ensure sustainable and efficient use of the subsurface. Albeit the impact on the groundwater quality is not the main concern in ATES planning, the impact is proved to be significant (Phernambucq, 2015). Studying this impact is needed to find optimal planning strategies based on thermal performance and managing the spreading of the contaminants.

This study aims at providing insight into the interaction between multiple ATES wells and contamination in order to quantify and predict the influence of the ATES systems. Therefore, the main objective of this research is to quantify the rate of spreading and dilution caused by high density ATES regions under various representative conditions. The research questions that this study focused on are:

1. To what extent do high density ATES regions influence contaminant spreading and dilution?
2. How do ATES systems interact in terms of external ATES transport?
3. How can enhanced spreading and dilution be managed, limited/mitigated and/or monitored?

1.3 Approach and structure of report

To answer the research questions, a generic study was performed. To be able to manage/monitor the enhanced spreading and dilution of ATES systems, the interaction between different systems is important to understand. Therefore, the interaction between two doublets is studied first. Thereafter, 4x4 well configurations are created to model the influence of larger ATES areas with a different well patterns and well densities. The parameters used in the models are based on the hydrogeological setting in the subsurface of Utrecht, since there is a lot of information available on this area. The numerical model created and used in the work of Jaxa-Rozen et al. (2015) enables studying the thermal interference in the subsurface. This model was also used in this study. Several adjustments are made to the model to make it suitable for studying contaminant transport. The most important adjustment is the method to model internal ATES transport.

In chapter 2, the literature relevant for this study is reviewed. This review covers both thermal performance and influence on contaminant spreading and dilution, as both factors are important in finding the optimal ATES application. In chapter 3 the methods used are described and explained. Followed by the results in chapter 4. This report concludes with the discussion and conclusion in chapter 5 and 6 respectively.

2 Literature review

In this chapter, the literature relevant for this study is reviewed. Starting with the working of ATES systems in section 2.1. Secondly, the thermal performance of ATES systems is explained in section 2.2, which is the main concern for ATES planning. In section 2.4, the influence of the ATES systems on the contaminated groundwater is described.

2.1 Working of ATES systems

ATES systems are used to sustainably heat and cool buildings. The operation of these systems is based on seasonal differences in thermal energy demand and supply. The surplus of thermal energy in summer is stored in the subsurface by a warm well and recovered in winter. The deficit in thermal energy in winter is stored in the subsurface by the cold well and is recovered in summer. Therefore, ATES systems are implemented in temperate climates with a balanced heating and cooling demand (Bloemendal, 2015). An ATES system needs at least two wells. When an ATES system consists of one cold and one warm well, it is called a doublet. When the heating and cooling demand are in balance, the ATES system is most efficient (Bloemendal et al., 2014).

The working of a low temperature ATES system is visualized in Figure 2.1 (Bloemendal, 2018). ATES systems are open systems, meaning that the water stored in the subsurface is in direct contact with the surrounding groundwater. In winter, water from the warm well is extracted and used to heat buildings. Afterwards the water is injected in the cold well. In summer, this system is reversed. Water from the cold well is extracted and used to cool buildings. Afterwards the water is injected in the warm well. For using the heat stored in the warm well, a heat pump is often used to further increase the temperature. This is needed for the heating systems to operate.

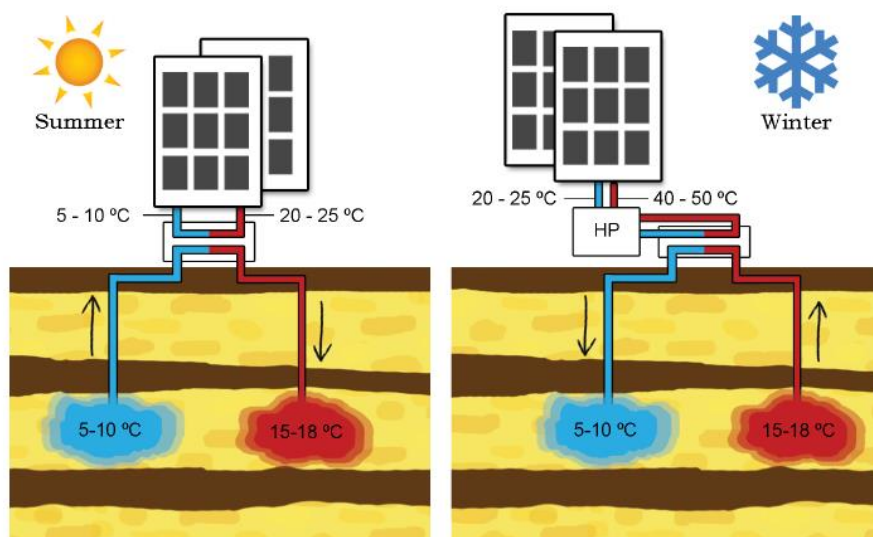


Figure 2.1 The working of an ATES system in The Netherlands (Bloemendal, 2018)

2.2 Thermal performance of an ATES system

The planning of ATES systems is mainly based on the thermal performance, since the goal of using ATES systems is minimizing emissions and provide sustainable heat. This performance is generally measured with the recovery ratio, which is defined as the volume of extracted water that has been injected in the former period, divided by the total extracted volume (Bear and Jacobs, 1965). This recovery ratio is influenced significantly by the well capture zone. When ambient flow velocities are small, the capture zone of a well is cylindrical and can be described with equation 1:

$$R_h = \sqrt{\frac{V_{season}}{\pi H \theta}} \quad (1)$$

With V_{season} the volume injected in one season [m^3]; H the filter length of the well [m] and θ the porosity of the aquifer [-].

However, when ambient flow velocities become larger, the capture zone changes location and becomes more ellipse. Bear and Jacobs (1965) defined a parameter \bar{t} to indicate the shape of the capture zone and the degree of deformation:

$$\bar{t} = \frac{2\pi D q^2 t_q}{\theta Q} \quad (2)$$

With \bar{t} the dimensionless parameter [-]; D the aquifer thickness [m]; q the specific discharge (from ambient flow) [m/day]; t_q the duration of injection or extraction [days]; θ the porosity [-] and Q the well discharge [m^3/day].

Equation 2 shows that the shape of the capture zone depends on the hydrogeological setting and the magnitude and duration of well activity. The higher the parameter \bar{t} , the more ellipse the capture zone and the lower the recovery ratio. A large well discharge can limit the effect of the ambient groundwater flow, since an increase in well discharge causes a decrease of \bar{t} . In addition, Bloemendal and Hartog (2018) found that the ratio between the area of the thermal zone and the injection volume A/V should be minimal to obtain higher thermal efficiencies. The smallest A/V values can be reached with high storage volumes.

According to Ceric and Haitjema (2005), equation 1 can be used to describe the capture zone when $0 \leq \bar{t} \leq 0.1$. For $0.1 \leq \bar{t} \leq 1$, the capture zone is still assumed to be circular, but displaced in the direction of the ambient flow. For larger values of \bar{t} , the capture zone is more ellipse and equation 1 does not hold.

2.3 Thermal performance of multiple ATES systems

The combined performance of multiple ATES systems does not only depend on the hydrogeological conditions in the subsurface, but also on the proximity of other ATES wells. Interference of the wells can have negative and positive effects on the recovery efficiency. When two wells of the same type interfere, the recovery efficiency increases, while two interfering wells of the opposite type results in a lower recovery efficiency for both wells. According to Duijf (2019), wells of the same type should be placed 0.5 times the thermal

radius apart and wells of opposite type should be placed more than 3 times the thermal radius apart. These distances provide the optimal thermal performance. Equation 3 describes the thermal radius of an ATEs well. Due to the heat transfer from the injected water to the soil particles, the thermal front is retarded when compared to the hydraulic radius (Figure 2.2):

$$R_{th} = \sqrt{\frac{V_{season}c_w}{c_{aq}\pi H}} \tag{3}$$

With R_{th} the thermal radius [m]; V_{season} the seasonal storage volume [m^3]; c_w the heat capacity of water [$J/m^3/K$]; c_{aq} the saturated heat capacity of the aquifer [$J/m^3/K$] and L the filter length [m].

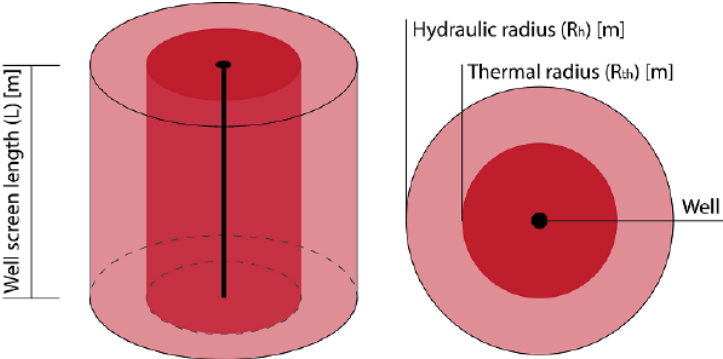


Figure 2.2 The difference between the hydraulic radius R_h and the smaller thermal radius R_{th} . The length of the cylinder is determined by the filter length of the well (Duijf, 2019).

This thermal radius is also used by policy makers to indicate the required distance between the wells. In the Netherlands, the required well distance between wells of the same type is $2R_{th}$ and for two wells of opposite type $3R_{th}$. This prevents negative interference between ATEs systems and also results in the clustering of wells of the same type (Calje, 2010). In Figure 2.3, the most common well patterns are visualized: line pattern and checkerboard pattern.

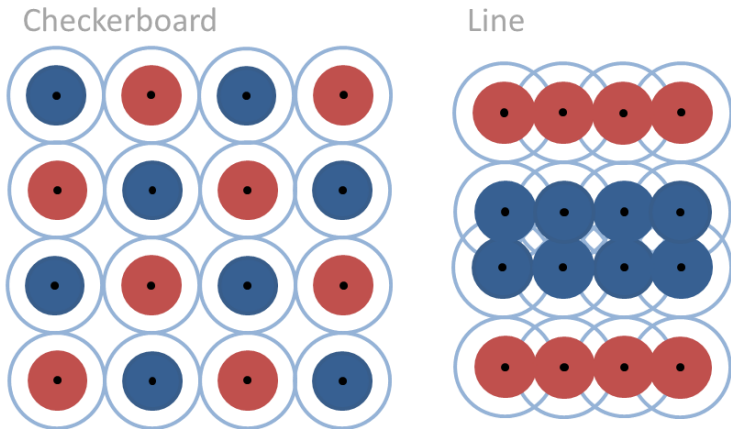


Figure 2.3 The two most common well patterns: checkerboard pattern and line pattern.

In literature, there is still some debate on the well configuration with the best thermal performance. Calje (2010) suggests that the line pattern performs best, because of the positive thermal interference. However, Li (2014) suggests that the occurrence of thermal bubbles in a line pattern cause the checkerboard pattern to be thermally optimal.

2.4 ATES induced spreading and dilution of contaminants

The placement of ATES systems in the subsurface causes the flow paths and temperature to change. A change in groundwater temperature can influence chemical reactions, the mobility of contaminants and biodegradation (MMB 3/4, 2012 ; Bonte, 2013). However, conventional ATES systems in The Netherlands are kept thermally balanced and the temperatures remain below 25 degrees. Therefore, the thermal effects on the chemical composition of the system are minimal and the effects that do occur are balanced by the other wells (Hartog, 2013 ; Tauw, 2010).

The hydrological effects are known to be of much larger influence on the groundwater composition (MMB 3/4, 2012). ATES systems cause complex flow patterns and thus influence the contaminant transport in multiple ways. The different mechanisms that influence the contaminated groundwater are explained in this section. The figures created by Phernambucq (2015) are used to support the explanation and illustrate the spreading and dilution mechanisms.

2.4.1 Well dilution

In practice, the composition and the conditions of the groundwater are not homogeneous throughout the whole aquifer and over the vertical profile. When water is extracted over the whole depth of the aquifer, it is mixed within the well and any vertical gradient is homogenized. In addition, when part of the extracted water is contaminated, the contamination is diluted by this mixing. These effects are visualized in Figure 2.4.

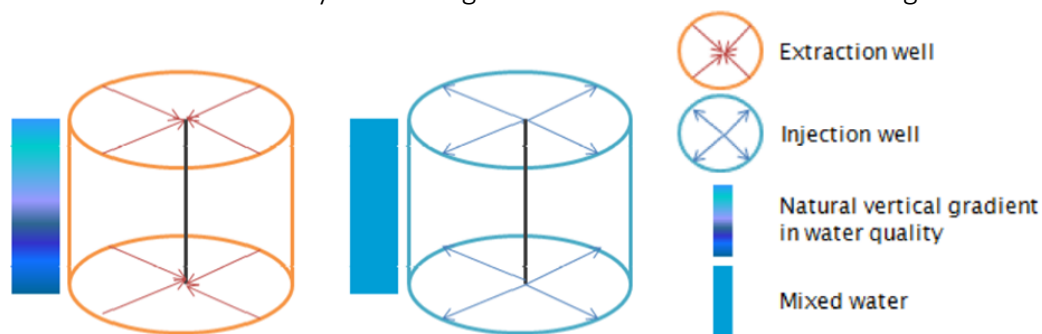


Figure 2.4 Well dilution, causing homogenising of natural vertical gradients and dilution of contaminants (Phernambucq, 2015).

2.4.2 Dispersive dilution

At the boundary of the injected water body, mixing by dispersion occurs (Figure 2.5). The injected water mixes with the surrounding water. When the ATES well starts extracting, some of the mixed/contaminated water will stay behind in the aquifer resulting in a lower contaminant load that is extracted, compared to injection. The magnitude of this effect depends on the flow velocities and the aquifer material properties like the dispersivity (Bloemendal and Hartog, 2018).



Figure 2.5 Mixing by dispersion at the boundary of the injected water volume (Phernambucq, 2015).

2.4.3 Internal ATES transport

In ATES systems, groundwater is extracted by a well and is simultaneously injected in the opposite well after heating or cooling a building. When this extracted groundwater contains contaminant mass, the contaminant moves to another location. In this study, this mechanism is called the internal ATES transport (Figure 2.6) and it increases contaminant spreading. Section 3.3.4 describes how this internal ATES transport is modeled. The amount of spreading that this mechanism causes depends on the distance between opposite wells and the amount of wells within an ATES system. In case an ATES system consists of multiple warm and cold wells, the extracted water volumes are mixed within the system before the water is redistributed over the opposite wells. Causing dilution within the system in addition to increased spreading. This internal spreading and dilution will always happen when an ATES system is implemented. The same goes for transport of contaminants between two wells of the same ATES system through the aquifer. Within the aquifer, transport of contaminants occurs between wells of the same ATES system as explained in section 2.3.5. This study does not focus on the internal ATES transport, since transport between wells of the same system is inevitable.

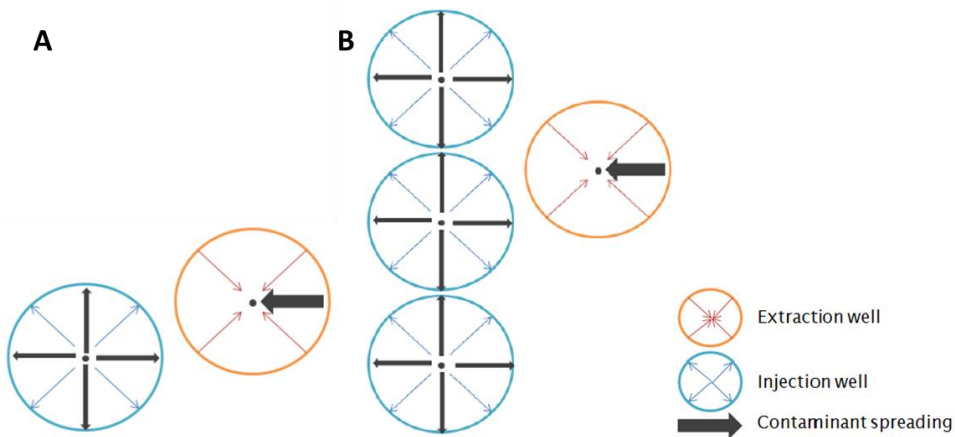


Figure 2.6 Spreading and dilution by internal ATES transport. A: Internal ATES transport in a doublet; B: Internal ATES transport in a system with multiple wells (Phernambucq, 2015).

2.4.4 Spreading by partial recovery

There are three processes that can cause only part of the injected water to be recovered again, resulting in contaminant that was pumped from one place in the aquifer to stay behind at another location as a result of internal ATES transport (section 2.3.3).

1. The first factor is dispersion, which always occurs. As described in section 2.3.2, dispersion causes water from the injected water body to enter the surrounding water. This water cannot be recovered, since it is not in the capture zone of the well anymore.
2. The second factor is ambient groundwater flow. Ambient groundwater flow causes the capture zone of the well to be displaced and/or elliptically shaped (Bear and Jacobs, 1965) and the injected water volume to be transported in the flow direction. This causes not all water that is injected to be extracted in the next season again. This way, injected water enters the surrounding groundwater and surrounding groundwater enters the capture zone of the well (Figure 2.7). The higher the well discharge, the smaller the influence of the ambient flow on the recovery of the well. The recovery ratio described in section 2.1 is a good indication of this mixing, since that ratio also depends on the shape of the capture zones. If the recovery ratio is low, the part of the water that is recovered is low and the spreading by partial recovery is large.



Figure 2.7 Partial recovery by ambient groundwater flow (Phernambucq, 2015).

3. The third factor is imbalance between the injection and recovery volume. For example when the cooling demand in summer is larger than the heating demand in winter. The volume of water used for cooling is larger and thus the volume stored in the warm well is larger. The amount of water needed to meet the heating demand in winter is in that case smaller than the stored volume. In this example contaminant will spread around the warm well, while the cold well is a net sink for contaminants.

2.4.5 External ATES transport

In an area with multiple ATES systems, there is hydrological interaction between these systems. When the capture zones of two ATES wells of opposite type overlap, contaminant mass can be transferred between those wells within one season (Figure 2.8), called short circuit flow. Without ambient groundwater flow, the capture zones overlap when the distance between the wells is equal to or smaller than $2R_h$. This is under the assumption that the stored volumes are perfect cylinders with a radius equal to the hydraulic radius. In practice, heterogeneities for example cause the cylinders to be imperfect. However, this simplification enhances the understanding of the system. As stated by Phernambucq (2015), when a minimal distance of $3R_{th}$ is applied between the wells, the capture zones overlap when $R_h \geq 1.5 * R_{th}$. The ratio between the hydraulic and thermal radius is described by equation 4:

$$x = \sqrt{\frac{c_{aq}}{c_w} \frac{1}{\theta}} \quad (4)$$

With x as the ratio between R_h and R_{th} [-]; c_{aq} the saturated heat capacity of the aquifer [$J/m^3/K$]; c_w the heat capacity of water [$J/m^3/K$] and θ the porosity [-].

As stated, when $x > 1.5$ the capture zones overlap and short circuit flow occurs. This mainly depends on the porosity and the heat capacity. A smaller porosity and higher heat capacity can cause the capture zones to overlap (more). In addition, ambient groundwater flow can alter the location and shape of the capture zones (Bear and Jacobs, 1965). This also influences overlap of capture zones.

Besides short circuit flow, spreading by partial recovery (section 2.3.3) can also cause the transport of contaminants over a period longer than one season. Partial recovery causes part of the injected volume to stay in the subsurface. The water that is not recovered again can enter the capture zone of another well of another ATES systems and be extracted by that well.

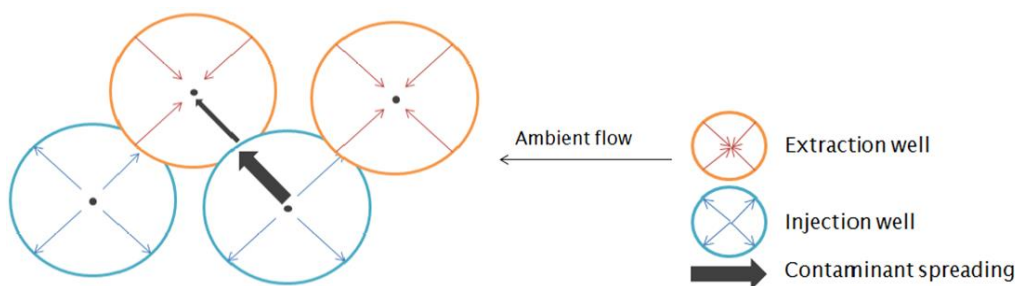


Figure 2.8 Connected capture zones which can cause transfer of contaminant mass between different ATES systems (Phernambucq, 2015)

2.4.6 Increased leaching from contaminant sources due to increased groundwater flow

Non aqueous phase liquids (NAPLs) are contaminants that are present in the subsurface in pure and dissolved form. When these pure contaminants are in the groundwater, they represent a constant contaminant source from which contaminants leach into the groundwater. This results in the formation of contaminant plumes in the downstream direction. The contaminant concentration in those plumes depend on the solubility of the NAPL, which is a property of the contaminant. When groundwater flow rates become larger, the supply of clean groundwater increases. This also increases the leaching from the contaminant source (Zuurbier, 2013).

With the implementation of ATES, the activity of the wells alter the hydraulic heads in the groundwater system and therefore also the groundwater flow. This effect is not restricted by the hydraulic radius, but extends much further (Bonte, 2013). In addition, when multiple ATES systems are placed together, the effect of the pump activity on the hydraulic head can be added using superposition. Resulting in larger head differences for line pattern configurations compared to checkerboard pattern configurations. The larger the hydraulic head differences, the higher the induced flow rates. These induced flow rates also increase leaching from contaminant sources. This increased leaching causes more contaminant mass to become part of the contaminant plume and thus more spreading. The extent of this influence mainly depends on the proximity of ATES wells to NAPLs.

3 Methods and materials

In this chapter, the modeling software is described first (section 3.1) followed by the used model, the model specifications and the model parameters (section 3.2). The research approach is explained in section 3.3. In the last section of this chapter (section 3.4), the assessment criteria are explained.

3.1 Modeling software

A numerical model was created with the SEAWAT software. This software is developed to model three-dimensional, variable density groundwater flow and multi-species transport (Langevin et al., 2008). SEAWAT makes it possible to combine MODFLOW and MT3DMS to calculate groundwater flow and contaminant and heat transport per time step. SEAWAT is operated through the FloPy package in Python. The FloPy package makes it possible to create, run and post-process MODFLOW-based models within a Python interface.

The code that is used to create, run and post-process the model and model results is based on the code used in the work of Jaxa-Rozen et al. (2015). The code was adjusted to make the model suitable for studying solute transport by implementing a method to model internal ATEs transport. This method makes sure that the mass that is extracted from the model by wells during time step A, is injected again in time step B. In section 3.2.4, this method is explained in more detail.

3.1.1 MODFLOW

MODFLOW is a freely available program that solves the three-dimensional groundwater flow equation (equation 5) with the finite difference method. This equation describes the calculation of the groundwater flux on the left hand side, which equals the storage and sources and sinks on the right hand side. The hydraulic head distribution and the water budget are the main MODFLOW results that are used as input for the contaminant transport. The wells are modeled with the well package incorporated in MODFLOW.

$$\nabla q = \nabla(K\nabla h) = S_s \frac{\partial h}{\partial t} - W \quad (5)$$

With q the specific discharge [L/T]; K the hydraulic conductivity [L/T]; h the hydraulic head [L]; S_s the specific storativity [$1/L$]; t the time [T]; W the sources and sinks [-].

The term $S_s \frac{\partial h}{\partial t}$ represents the amount of water stored in the porous medium over time. This term is equal to the groundwater flux when it is combined with the sources and sinks (W). As the calculations in this study are done in steady state, S_s is inactive.

3.1.2 MT3DMS

The Modular Transport Three-Dimensional Multi-Species (MT3DMS) model, is used to model contaminant and heat transport. This model simulates advection, dispersion, adsorption and chemical reactions with the results of the MODFLOW model as input. The output of MT3DMS is used in multiple ways, as described in the assessment criteria (section 3.4). The transport equation is based on the conservation of mass (Zheng, 2010):

$$R \frac{\delta(\theta C)}{\partial t} = \left(1 + \frac{\rho_b}{\theta} K_d\right) \frac{\delta(\theta C)}{\partial t} = \nabla * (\theta D_{tot} * \nabla C) - \nabla * (qC) + q_s C_s \quad (6)$$

With R the retardation factor [-]; θ the porosity [-]; C the concentration of the solute [M/L^3]; t the time [T]; ρ_b the bulk density [M/L^3]; K_d the distribution coefficient [L^3/M]; D_{tot} the dispersion coefficient [L^2/T]; q the specific discharge [L/T]; q_s the volumetric flow rate per unit volume of aquifer representing fluid sources or sinks [$1/T$]; C_s the concentration of the fluid source or sink [M/L^3].

The left hand term $R \frac{\delta(\theta C)}{\partial t}$ describes the retardation of the contaminants caused by adsorption by the porous medium. The right hand side consists of three different terms. The first term $\nabla * (\theta D_{tot} * \nabla C)$ represents the hydrodynamic dispersion that consists of diffusion and mechanical dispersion. The second term $\nabla * (qC)$ represents the advection and the third term $q_s C_s$ represents sources and sinks. An example of a source and sink in this study are the wells. Degradation can be added to the equation as a fourth term on the right hand side.

While this study focuses on the transport of contaminants, it is also important to note that the heat transport can be modeled with MT3DMS since the equations are mathematically identical (Equation 7) (Zheng, 2010):

$$R_T \frac{\delta(\theta T)}{\partial t} = \left(1 + \frac{\rho_s K_{dtemp}}{\theta}\right) \frac{\delta(\theta T)}{\partial t} = \nabla * (\theta D_{Ttot} * \nabla T) - \nabla * (qT) + q_s T_s \quad (7)$$

The left hand term $R_T \frac{\delta(\theta T)}{\partial t}$ represents the retardation of the heat front caused by transfer of heat from the groundwater to the solid particles in the soil. On the right hand side, the first term $\nabla * (\theta D_{Ttot} * \nabla T)$ represents the thermal dispersion, which consists of heat transport by conduction and mechanical dispersion. The second term $\nabla * (qT)$ represents the heat transport by convection and the third term $q_s T_s$ represents the sources and sinks.

3.1.3 SEAWAT

As mentioned above, SEAWAT uses MODFLOW and MT3DMS to model three-dimensional, variable density groundwater flow and multi-species transport (Langevin et al., 2008). Equation 8 is solved with SEAWAT:

$$\nabla * \left[\rho_f \frac{\mu_0}{\mu} K_0 \left(\nabla h_0 + \frac{\rho_f - \rho_0}{\rho_0} \nabla z \right) \right] = \rho_f S_{s,0} \frac{\partial h_0}{\partial t} + \theta \frac{\partial \rho_f}{\partial C} \frac{\partial C}{\partial t} - \rho_s q'_s \quad (8)$$

With ρ_f the fluid density [M/L^3]; μ_0 the dynamic viscosity at a reference concentration and temperature [M/LT]; μ the dynamic viscosity [M/LT]; K_0 the hydraulic conductivity of the material when saturated [L/T]; h_0 the hydraulic head measured at a reference concentration and temperature [L]; ρ_0 the fluid density at the reference temperature and concentration [M/L^3]; z the elevation head [L]; $S_{s,0}$ the specific storativity [L]; t the time [T]; ρ_s the density of the source and sink [M/L^3].

3.2 Model specifications

3.2.1 Model parameters

The parameters used in the model are based on measurements in the subsurface of the city center of Utrecht. This location was chosen because there is a relatively large amount of information available (MMB9, 2012 ; Tauw, 2010 ; Deltares, 2009) and there are a lot of ATES systems active in this area. The results of this study can therefore be tested and compared with Utrecht as a real life case study. Due to time limitations, this case study is not part of this thesis. In Table 3.1 , the values of the hydrogeological and transport parameters are shown. Table 3.2 shows the parameters that are used for the temperature and contaminant species.

Parameter	Value	Unit
Porosity (θ)	0.25	[-]
Horizontal conductivity (K)	30	m/day
Vertical conductivity (K_v)	6	m/day
Specific storativity (S_s)	0.00001	m^{-1}
Density solids (ρ_s)	2640	kg/m^3
Density water (ρ_f)	1000	kg/m^3
Courant number	0.8	[-]
Dispersivity (α)	0.5	m

Table 3.1 Hydrogeological and transport parameters (MMB9, 2012 ; Tauw, 2010 ; Deltares, 2009).

Parameter	Temperature	Contaminant
Adsorption	Linear sorption	No sorption
Distribution coefficient [m^3/g]	$1.697 * 10^{-3}$	-
Diffusion coefficient [m^2/day]	0.117321	$1.0 * 10^{-10}$

Table 3.2 Species specific used parameters.

During this study, the model was adjusted to obtain smaller run times. This was done by downscaling the model. Therefore, the model specifics in Table 3.3 are shown for both model versions. The initial model consisted of one aquifer between two aquitards. Since the transport of the contaminants towards the aquitards and variations over the depth of the aquifer are not taken into account, the aquitards were removed and the aquifer thickness reduced. It is important to note that the variables which represent a size or a volume are also scaled to the new and smaller model. Besides the parameters in Table 3.3 , the set up and all other parameters are kept constant between the two model versions.

During the downscaling of the model, an error was discovered. The concentration in the aquitards was set to be constant and had a value of 1 g/L. This error probably influenced the results for the 2x2 well configurations. However, the mass balance was stable, the fictitious initial concentration was 100 g/L and the thickness of the aquifer was relatively large. Therefore, the influence of this error is negligible.

Variables	Initial model	Downscaled model
Number of layers	3 (2 aquitards, 1 aquifer)	1 (1 aquifer)
Aquifer thickness	30 m (6 layers of 5m)	10 m (2 layers of 5m)

Aquitard thickness	10 m (2 layers of 5 m)	-
Well discharge	85000m ³	21250m ³
Filter length wells	30 m	10 m
Well radius	0.3 m	0.3 m
Thermal radius (Rth)	32 m	32 m
Hydraulic radius (Rh)	52 m	52 m

Table 3.3 Model specifics based on information from MMB9 (2012), Tauw (2010) and Deltares (2009) for the two different model versions.

The well discharge in Table 3.3 is distributed over the season with a sine function. The well discharge distribution is shown in Figure 3.1. The boundaries of the models have a constant head. When adding ambient groundwater flow, the constant head values at these boundaries are adjusted to create the specific discharge in the model.

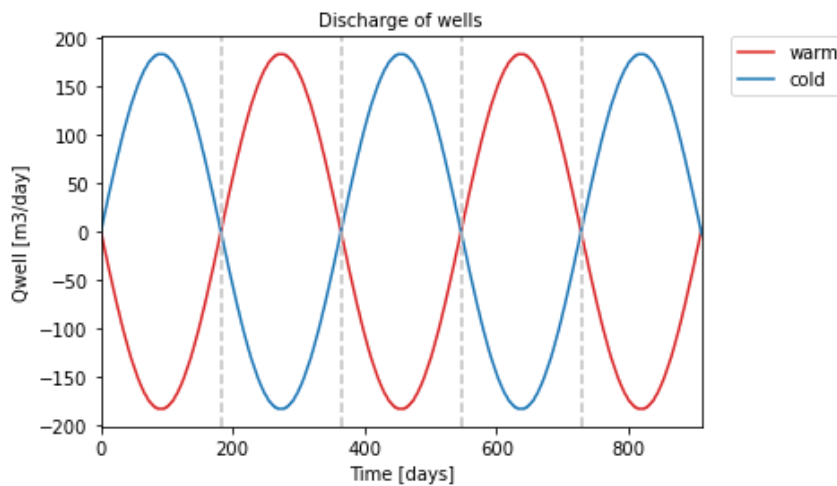


Figure 3.1 The sine discharge distribution of the warm and cold wells in the model.

3.2.2 Model discretization

The assessment criteria, which are described in section 3.4, were used to determine the time steps and the grid size. The resolution in time and space was increased until the higher resolution did not influence the results anymore. This resulted in time steps of 1 day and grid sizes of 2x2m. The results used to determine this discretization are shown in Figure 3.2 and Figure 3.3.

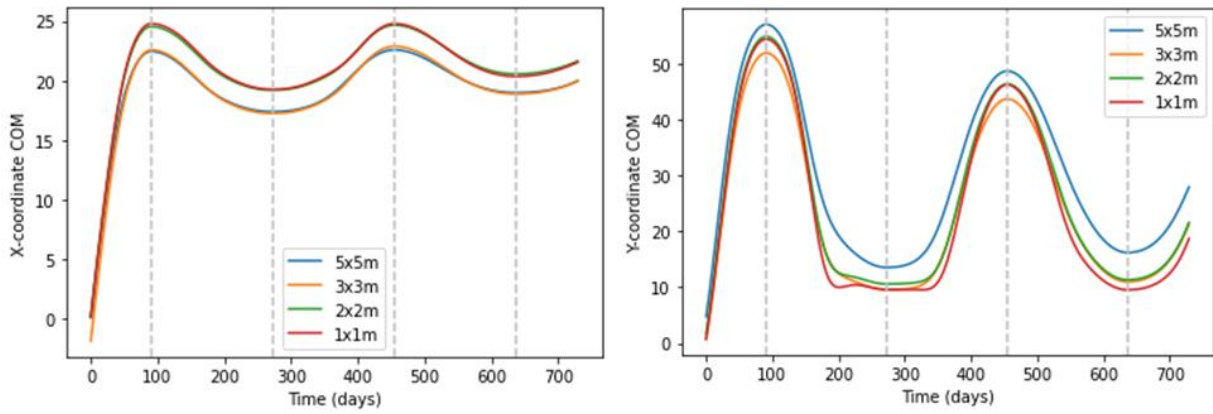


Figure 3.2 The center of mass results for different grid sizes to determine the spatial resolution.

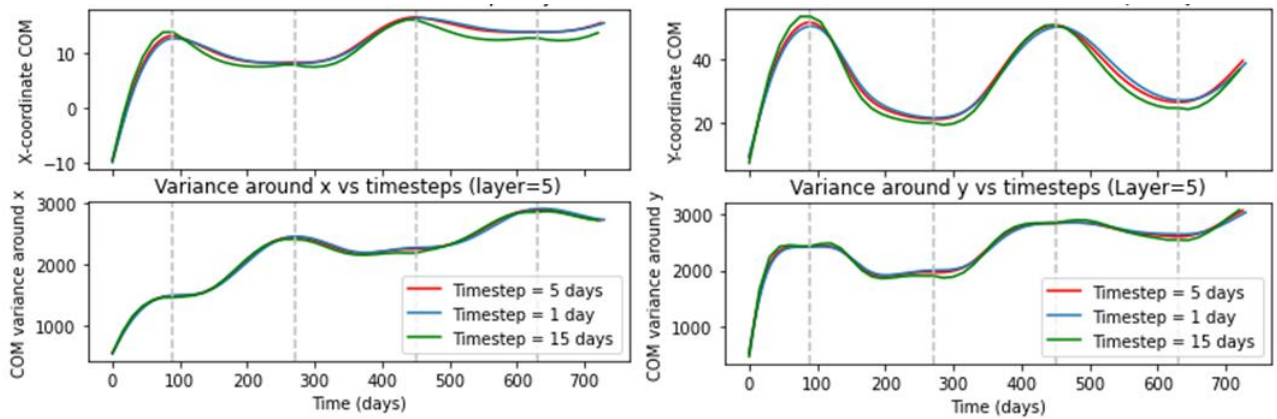


Figure 3.3 The center of mass results for different grid sizes to determine the temporal resolution.

In Figure 3.4, the grid of the model is shown. The grid cells around the wells are equal in size, while the size of the grid cells increase logarithmically with increasing distance from the well framework. The parameters shown in Figure 3.4 are defined in Table 3.4. These parameters show that the distance between the wells and the model boundaries is at least 700 meters. The total modeled area differs per scenario and depends on the area that the modeled wells are in. The more wells and the larger the distance between the wells, the larger the model becomes. In Table 3.4, the vertical resolution dz is also specified. Since this study does not consider variation over the depth of the aquifer, this resolution is of less importance and a value of 5 m will suffice.

Parameters	Value [m]
dmin	2
dmin_bound	200
Around_all	500
dmax	250
dz	5

Table 3.4 The parameters determining the discretization and extent of the model as defined in Figure 3.4.

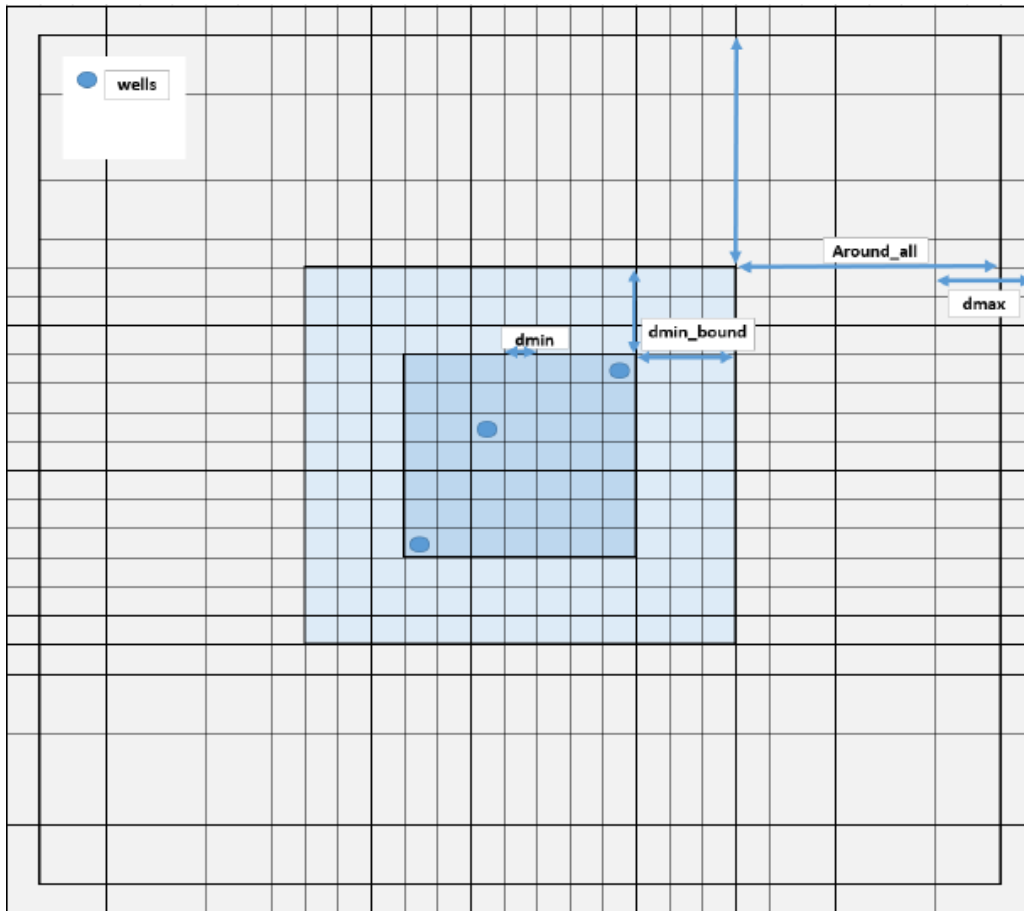


Figure 3.4 The grid structure and parameters used in this study.

3.2.3 Modeled contaminant

A trace contaminant is used in this study, meaning that the contaminant does not adsorb or degrade. The contaminant is introduced in the model by one of the injecting wells during the first 40 days of the model run. This timeframe is chosen because there is no internal or external ATES transport of contaminants detected in the four scenarios within these first 40 days. During this period, a fictitious concentration of 100 g/L is assigned to the injected water. Meaning that, for the initial model, the first 9966 m^3 water contains a concentration of 100 g/L. The total mass in the system is thus equal to 996.6 kilograms. For the downscaled model, the first 2493 m^3 water contains a concentration of 100 g/L. This corresponds to a total mass of 249.3 kilograms.

The initial contaminant mass is thus present in the capture zone of one ATES well and is subject to the working and interaction of all ATES wells. It is therefore very suitable for studying spreading and dilution mechanisms by and between the ATES systems.

3.2.4 Internal ATES transport

The used model code is originally made to model the heat that is stored by the ATES systems (Jaxa-Rozen et al., 2015). This heat transport is modeled with MT3DMS as explained in section 3.1.2. In this model, the temperature of the water that is injected in a certain well is assumed to be constant within one season and between seasons. That is why the extracted and injected water of an ATES system are not linked. To make the script suitable for looking at

contaminant transport, this link is needed to redistribute the contaminant mass that has been extracted by ATES wells. Therefore, besides the addition of a second species, the following internal ATES transport method was defined:

1. Calculation of extracted mass per well: After the calculation of time step A, the concentration at the location of the extracting wells is calculated. This is done by averaging the concentration over the whole depth/different layers of the aquifer. This average concentration is multiplied with the discharge of the same well in time step A. This results in the extracted mass per well.
2. Calculation of extracted mass per system: If there are ATES systems in the model which consist of more than one extraction well (in time step A), the extracted masses of those wells are added. Resulting in the total extracted mass per ATES system.
3. Calculation of injection concentration: The total extracted mass per ATES system is divided by the injection volume of that ATES system in time step B. This way, the injection concentration for time step B is calculated and assigned. Meaning that the contaminant concentration in the water, injected by different wells that belong to the same ATES system, are equal.

The mass budget of the system was used to test this method.

3.3 Research approach

In order to answer the research questions identified in chapter 1, the interaction between different ATES systems and contaminant transport are studied in detail. That is why 2 doublets in a 2x2 well configuration are created first. Throughout the research approach, the distance in terms of thermal radius and hydraulic radius (Equations 1 and 3) are both taken into account. When studying the interaction between doublets with respect to contamination, the distances are mainly expressed as a function of the hydraulic radius since this radius represents the front of the water body and thus the front of contaminated or clean groundwater. However, the scenarios are not based on the hydraulic radius, but on policy and practice situations. Table 3.5 shows the details of the scenarios used. The low density scenarios are based on the policy that wells of the same temperature should be $2R_{th}$ ($1.23R_h$) apart and wells of the opposite temperature should be $3R_{th}$ ($1.85R_{th}$) apart to avoid negative thermal interference. According to Li (2014), these distances are somewhat overdone since the thermal efficiency only increases with increasing well distance up until $2.5R_{th}$. Li (2014) shows that a well distance of $2R_{th}$ already reaches an efficiency of higher than 70%. In addition, in areas with a high ATES demand, the wells of the same type are often clustered to enlarge the thermal efficiency and the efficient use of the subsurface space. This causes the same type of wells to be much closer than the policy distance (Tauw, 2010). Therefore, the distance between wells of the same temperature are $1R_{th}$ ($0.6 R_h$) apart and wells of opposite temperature are $2R_{th}$ ($1.23R_h$) apart in the high density scenarios.

Scenarios	Distance between wells with same temperature	Distance between wells with opposite temperature	Well pattern	Wells per area (wells/m ²)
High Density Line (HDL)	1 Rth / 0.6 Rh	2 Rth / 1.23 Rh	Line	4.9
Low Density Line (LDL)	2 Rth / 1.23 Rh	3 Rth / 1.85 Rh	Line	1.6
High Density Checkerboard (HDC)	1 Rth / 0.6 Rh	2 Rth / 1.23 Rh	Checkerboard	2.4
Low Density Checkerboard (LDC)	2 Rth / 1.23 Rh	3 Rth / 1.85 Rh	Checkerboard	1.1

Table 3.5 The definition and distances between the wells for the four main scenarios.

3.3.1 2x2 well configurations

The 2x2 well configurations are used to study the influence of doublets on the spreading and dilution of contaminants and the external ATES transport. The models are run for 2.5 years, which is enough time for the contaminant to be transferred through the whole system.

3.3.1.1 Interaction between two doublets in line pattern

Figure 3.5 shows the set-up of two doublets in line pattern. First, the high and low density (HDL and LDL) scenarios are run in order to gain knowledge on the spreading and dilution caused by this well pattern.

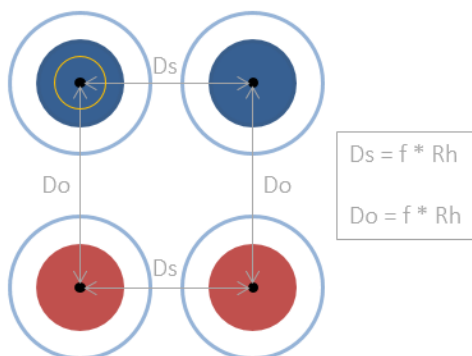


Figure 3.5 The 2x2 line configuration showing the definition of the distance between the wells with the same temperature (D_s) and the distance between the wells with the opposite temperature (D_o). The red wells are warm and the blue wells are cold. The yellow circle marks the well in which the initial contamination is injected.

Varying well distances

Secondly, the well distance between the same (D_s) and opposite (D_o) thermal wells is varied (Figure 3.5). Preliminary results showed that two mechanisms cause external ATES transport between two doublets in line pattern: (1) dispersion causes mass transfer between two wells with the same temperature and (2) short circuit flow causes mass transfer between opposite wells (chapter 4):

- To study external ATES transport by dispersion, the distance D_s between the same wells is varied between $1.5R_h$ ($2.4R_{th}$) and $0.86R_h$ ($1.4R_{th}$). The distance D_o between the opposite wells is set to $1.85R_h$ ($3R_{th}$) to minimize the influence of the opposite wells.
- To study the external ATES transport by short circuit flow, the distance D_o and D_s are varied with the HDL scenario as the reference situation. D_o was varied between $1R_h$ ($1.6R_{th}$) and $2R_h$ ($3.25R_{th}$) and D_s was varied between $0.5R_h$ ($0.8R_{th}$) and $1.23R_h$ ($2R_{th}$).

Varying dispersivity

The dispersivity value used in the models is 0.5 m and represents the situation in the city center of Utrecht. To study the influence of dispersivity on the external ATES transport between the same type of wells, the dispersivity value was varied between 0.0 and 2.0 meters. These values were chosen since they are well within the scope of dispersivity values measured in field experiments (Gelhar, 1992).

Differences in well discharge between two ATES systems

The high density scenario (HDL) is also used for studying the effect of differences in well discharges between the doublets. The discharge of the left doublet is kept constant at 85000 m^3 , which is the average ATES system size in the city center of Utrecht. The discharge of the right doublet, which was initially clean, is varied between half and twice the average volume: 42500 m^3 and 170000 m^3 .

3.3.1.2 Interaction between two doublets in checkerboard pattern

Figure 3.6 shows the set-up of two doublets in checkerboard pattern. For this well configuration, the high and low density (HDC and LDC) scenario are also run to understand the spreading, dilution and mass transfer between the two doublets.

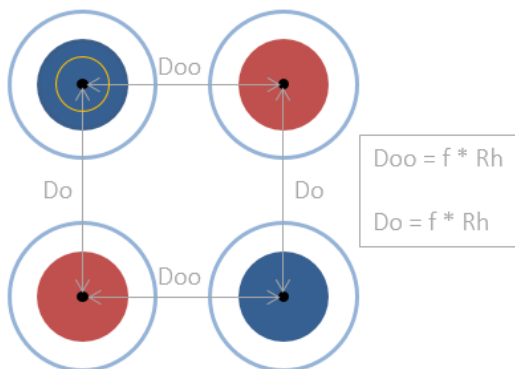


Figure 3.6 The 2x2 checkerboard configuration showing the definition of the distance between two wells with opposite temperature within the same doublet (D_o) and the distance between the wells with opposite temperature and opposite doublet (D_{oo}). The red wells are warm and the blue wells are cold. The yellow circle marks the well in which the initial contamination is injected.

Varying well distances

The distance between opposite wells of opposite ATES systems (D_{oo}) is varied for this configuration between $1R_h$ ($1.6R_{th}$) and $3R_h$ ($4.8R_{th}$). These values are chosen because the doublets are at a distance of $1.23R_h$ ($2R_{th}$) in the high density scenario and because the flow between the wells is expected to occur at distances larger than $2R_h$ ($3.25R_{th}$).

3.3.2 Influence of ambient groundwater flow on the 2x2 well configurations

The ambient groundwater flow is added to the four scenarios: HDL, LDL, HDC, LDC (Table 3.5). First, a groundwater velocity of 10 m/year is chosen, since that velocity is representative for the situation in the city center of Utrecht (Tauw, 2010). The results are used to understand the influence of ambient groundwater flow on the contaminants. Secondly, the ambient groundwater flow is varied between 5 and 20 m/year for the two high density scenarios (HDL and HDC) to study the influence of higher and lower velocities. The direction of the ambient flow is shown in Figure 3.7 and is the same for all scenarios throughout this study.

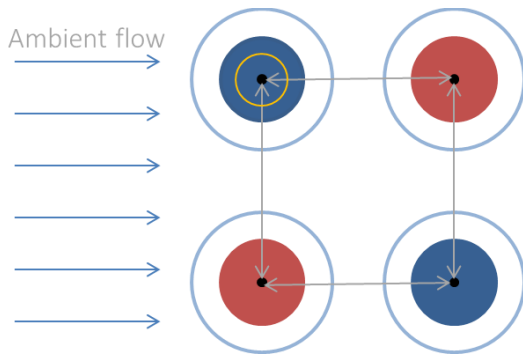


Figure 3.7 The direction of the ambient groundwater flow with respect to the wells.

3.3.3 4x4 well configurations

The 4x4 well configurations are created to study the influence of a field of wells with a certain well density on the contaminant spreading and dilution. The goal of these configurations is to obtain results which can be extrapolated to larger regions with the same wells density. Again, this configuration is considered for four different scenarios: HDL, LDL, HDC and LDC (Table 3.5). The models are run for 10 years. In practice, ATES systems operate during 30 or 40 years. However, in order to limit the influence of the boundaries of the well configurations, a runtime of 10 years was chosen. This period is sufficient to observe trends in spreading and dilution. In Figure 3.8 and Figure 3.9 the set-up of the two well patterns are visualized. First, the models are run without ambient groundwater flow.

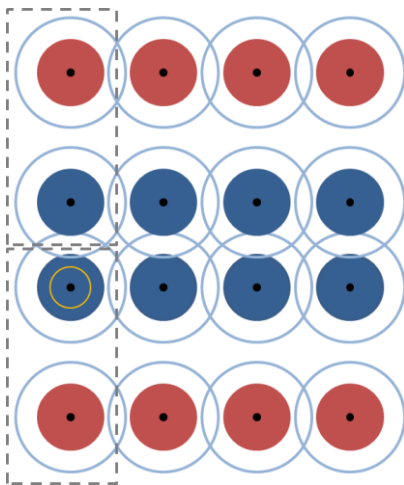


Figure 3.8 The low density 4x4 line well configuration (LDL). The yellow circle marks the well in which the initial concentration is injected. The well framework consists of 8 ATES systems / 8 doublets. How these systems are aligned is shown with the grey boxes.

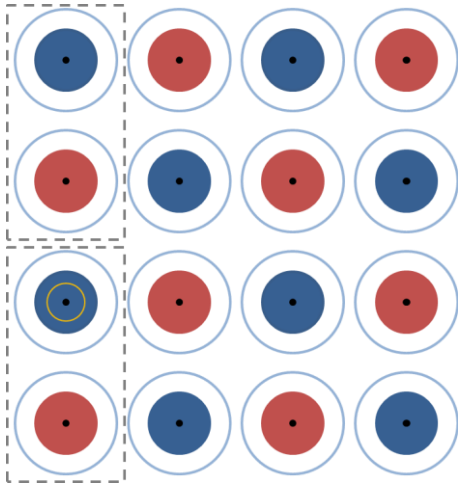


Figure 3.9 The low density 4x4 checkerboard well configuration (LDC). The yellow circle marks the well in which the initial concentration is injected. The well framework consists of 8 ATEs systems / 8 doublets. How these systems are aligned is shown with the grey boxes.

Ambient groundwater flow

Ambient groundwater flow with a velocity of 10 m/year is added to the four main scenarios. A reference plume is created to compare the spreading and dilution by the wells with the spreading and dilution by the ambient flow. The LDL scenario is used during the formation of the reference plume. During the 40 days in which the initial plume is created, cold wells are injecting and warm wells are extracting. After these 40 days, all the wells are turned off. In section 3.2.3, the formation of the initial concentration is explained.

3.4 Assessment criteria

3.4.1 Center of mass and variance

Assessment criteria are formulated in order to interpret and analyze the results. To identify the location and the spreading of the contaminants, the center of mass and the variance are used. The center of mass shows the center of the contaminant plume and is therefore used to describe the location and movement of the contaminant plume. The variance shows the distribution of the contaminant concentration with the center of mass as the reference point. The variance is therefore used as a measure for the spreading and dilution. In equations 9, 10 and 11, the mathematical definitions are shown with the parameter of interest being the contaminant concentration (B.H. Kueper and E.O. Frind, 1991). The results are also obtained for the z-direction, but these results are not used in this study since there is no variation in the z-direction in the used model. In practice, variation in the z-direction does occur.

$$M_{ij} = \int_{-\infty}^{\infty} \int_{-\infty}^{\infty} C(x, y) x^i y^j dx dy \quad (9)$$

$$COM: \quad x = \frac{M_{10}}{M_{00}} \quad \text{and} \quad y = \frac{M_{01}}{M_{00}} \quad (10)$$

$$Variance: \quad \sigma_{xx}^2 = \frac{M_{20}}{M_{00}} - x^2 \quad \text{and} \quad \sigma_{yy}^2 = \frac{M_{02}}{M_{00}} - y^2 \quad (11)$$

The smaller the variance, the closer the majority of the mass to the center of mass. When the variance is larger, the contaminants are further away from the center of mass and thus more spread over the aquifer. However, not only the distance of the contaminant mass is considered, the amount of mass is also taken into account. For example, consider two situations in which the contaminant mass and the plume area are equal. The variance will be higher for a plume in which the contaminant is spread evenly compared to a situation in which the contaminant concentration is highest at the center and decreases towards the boundaries.

3.4.2 Plume area

The plume area is also an important assessment criteria and an addition to the variance. The plume area can be used to visualize the extent of the spreading and to determine the moment in time at which another ATES system is contaminated. To determine this area, a threshold concentration needs to be chosen in order to eliminate the effect of numerical dispersion and thus to get reliable results. In Table 3.6, several contaminants can be found with their solubility and intervention values. The factor column shows the factor of difference between these two. This factor is also used to calculate the threshold concentration in this study. The fictitious concentration of 100 g/L is considered to be equal to the solubility, which leads to the model threshold concentrations displayed in the last column.

Contaminant	Solubility (g/L)	Intervention value ($\mu\text{g/L}$)	Factor (-)	Model threshold concentration (g/L)
Benzene	1.79	30	$1.7 * 10^{-5}$	0.0017
PCE	0.15	40	$2.7 * 10^{-4}$	0.027
TCE	1.1	500	$4.5 * 10^{-4}$	0.045
DCE	0.8	20	$2.5 * 10^{-5}$	0.0025
VC	1.1	5	$4.5 * 10^{-6}$	0.00045

Table 3.6 Solubility and intervention values for different contaminants and the factor used to calculate the threshold concentration in the model.

To incorporate a bandwidth of different intervention values, the largest and smallest values (for PCE and VC) are both used in calculating the plume areas. This is valuable since it is known that VC is abundantly present in the subsurface of Utrecht (MMB 9, 2012). In addition, this is a way to incorporate the importance of choosing a lower boundary. The observed trends in this study are equal for both threshold concentrations, confirming that both values will give reliable results.

3.4.3 Normalization

The scenarios compared in this study consist of the same amount of wells which are placed at different distances. These different distances between the wells influence the results. To compare the results based on the well density or to eliminate the influence of the well distance, the results are normalized. The center of mass and variance results are generated in one direction. Therefore, the results can be normalized with the well distance in that same direction. Equation 12 and 13 show the normalization in the x-direction:

$$COM_{normalized}(x) = \frac{COM(x)}{L_x} \quad (12)$$

$$VAR_{normalized}(x) = \frac{VAR(x)}{L_x} \quad (13)$$

With $COM(x)$ the center of mass in the x-direction [m]; L_x the distance between the doublets (D_s or D_o) [m] and $VAR(x)$ the variance in the x-direction.

The plume area is also normalized with the area occupied by the wells (Equation 14). The resulting relative spreading shows the amount of spreading (m^2) per m^2 starting area within a certain well density:

$$Relative\ spreading = \frac{A_{plume}}{D_s * D_o} \quad (14)$$

With A_{plume} the plume area [m^2]; D_s the distance between the same wells of opposite ATES systems [m]; D_o the distance between the opposite wells of the same ATES system [m].

3.4.4 Output concentrations

The UCN-files produced by MT3DMS contain the concentration per grid cell. These files are used to make contour plots which show the distribution of the contaminants in the subsurface. This is mainly used to visualize the results and increase the understanding of the systems.

The contaminant concentrations at the locations of the wells are also obtained from these files, stored and used. These concentrations are calculated by averaging the values at the well coordinate over the whole depth of the aquifer. In this study, there is no variation in the z-direction, so this average concentration is equal to the concentration anywhere in the vertical profile. These concentrations are mainly used for the internal ATES transport method (section 3.2.4), to document the moment at which ATES systems are contaminated and to analyze the amount of external mass transport.

4 Results

In this chapter, the results are presented following the structure of the research approach (section 3.3) and analyzed.

4.1 Interaction between two doublets in line pattern

4.1.1 Description of observed plume development

The spreading of the contaminant by two line pattern doublets is visualized in Figure 4.1. In this well configuration, the two top wells extract and inject water at the same time and the two bottom wells extract and inject water at the same time. This causes the sharp interface between the contaminated volume of water injected by the top left well and the clean volume of water injected by the top right well. The black dots in Figure 4.1 represent the center of mass, which shows the location and movement of the contaminant plume as a whole as explained in section 3.4.1. Since the flow of both top wells counteract each other, the injected water volumes do not become cylindrical. Instead, the injected water volume extends in the opposite direction, away from the interface between the two water bodies. This results in the initially contaminated water, which is injected in the top left well, to move to the left. Therefore, the center of mass also directly moves to lower x-values and roughly stays there.

Figure 4.2 shows that the movement of the center of mass depends on the distance between the two doublets (D_s). The top left graph shows the x-coordinate of the plume location and the bottom left graph shows the variance in the x-direction. When the doublets are placed closer together, the contaminant plume moves further to the left. This movement probably causes spreading due to partial recovery to increase. In the bottom right graph, the normalized results show that the variance, which indicates spreading and dilution, is indeed larger when the distance between the doublets is smaller. The variation through time in both graphs is caused by the attraction of the contaminant towards the well when the discharge of the well switches from injecting to extracting water and vice versa.

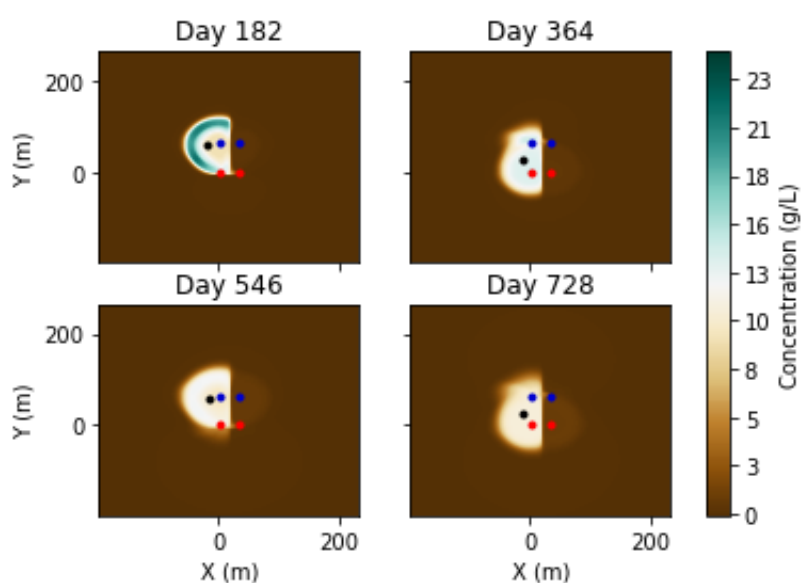


Figure 4.1 Contour plots of the contaminant distribution after 182, 364, 546 and 728 days. Generated with the 2x2 high density line (HDL) scenario. The black dot marks the location of the center of mass.

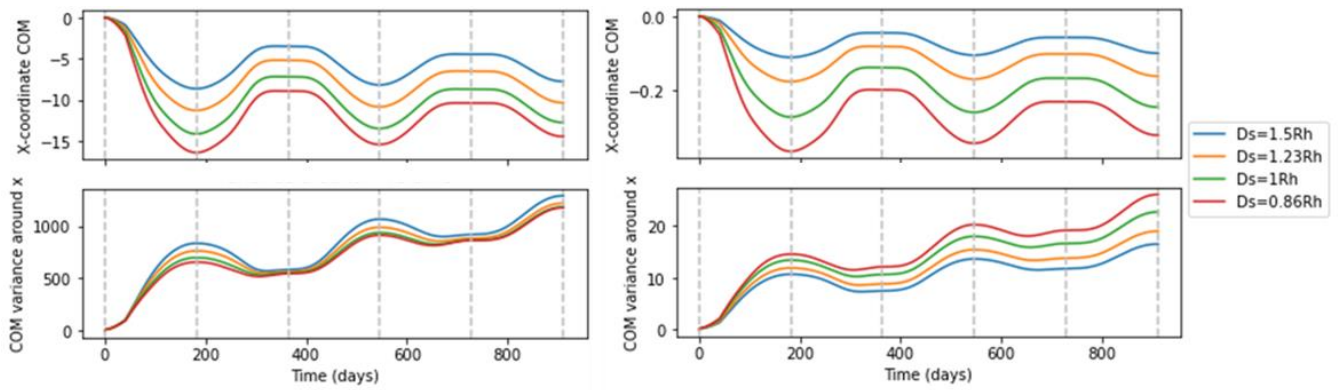


Figure 4.2 Left: the location of the center of mass (m) and the variance in the x -direction. Right: The same results normalized for the changing well distances. $Do=1.85Rh$.

4.1.2 External ATES transport in line pattern

As described in section 3, the external ATES transport refers to the transport between two different ATES systems. Between two doublets in line pattern, the transport is studied by looking at the concentration detected through time in the wells of the right doublet, which is initially clean.

Short circuit flow

To test if external ATES transport by short circuit flow occurs, the contaminant concentration in the bottom right well was measured in the first season. Figure 4.3 shows that this short circuit flow occurs between doublets in line pattern in the high density scenario (orange graph). Meaning that within one season, the contaminated water injected in the top left well flows towards the bottom right well. If short circuit flow occurs and how high the concentrations are depends on the distance between these wells. This distance depends on both the distance between the wells within the same ATES system (Do) and the distance between the wells of different ATES systems (Ds). Figure 4.3 shows that short circuit flow only occurs when the distance between the opposite wells of the different ATES systems is relatively small. This short circuit flow thus does not occur in the low density scenario.

In the high density scenario (orange line), the concentrations found in well 2 are approximately a factor 35 higher than the average threshold concentration calculated in section 3.4.2. This shows the significance of this external ATES transport.

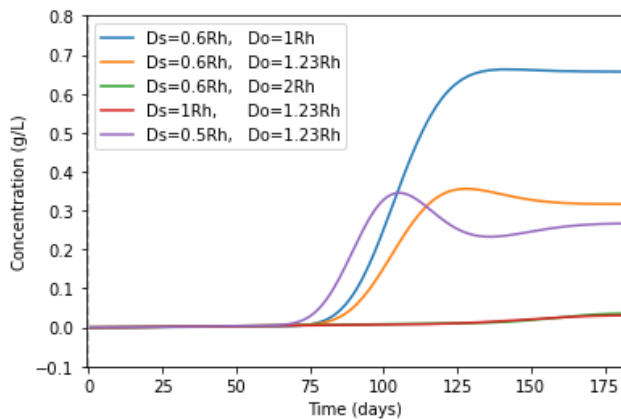


Figure 4.3 Contaminant concentrations measured in the bottom right well during the first season for different distances between the wells (Ds and Do).

Differences in well discharges between ATES systems

Figure 4.4 shows the influence of the differences in well discharge between doublets on the external ATES transport by short circuit flow. The discharge of the left doublet is kept constant at 85000 m^3 and the discharge of the right doublet is varied between 42500 m^3 and 170000 m^3 . The blue line shows the scenario in which both discharges are equal. This figure shows that the external ATES transport by short circuit flow increases with increasing difference between the well discharges. The yellow and green line represent the scenario in which the discharge of the left doublet is smaller than the discharge of the right doublet. The red line represents the scenario in which the discharge of the left doublet is larger than the discharge of the right doublets. Since smaller volumes of water are pumped in the scenario represented by the red line, the mass transfer occurs later. The yellow and green line show that the mass transfer occurs earlier when the discharge of the right doublet is increased. This makes sense since pumping of larger volumes of water increases the flow between the wells.

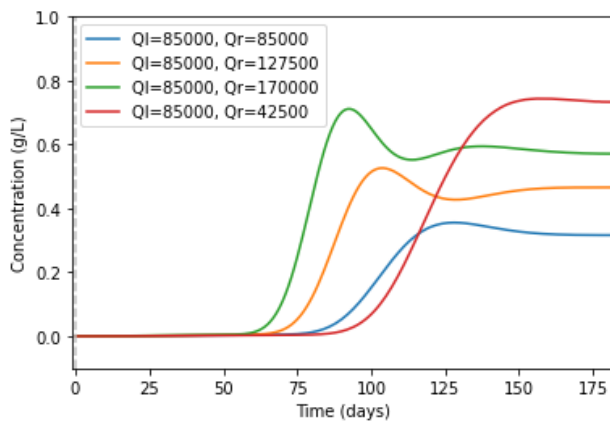


Figure 4.4 The concentration in the bottom right well for different doublet discharges. The blue line represents the mass transfer for the high density line (HDL) scenario with equal discharges.

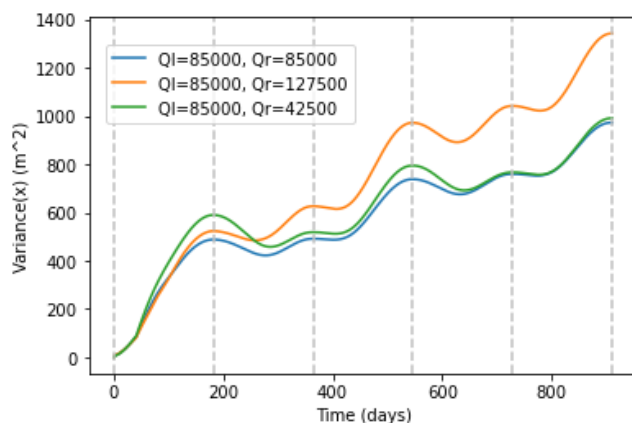


Figure 4.5 Variance (x) results for differences in well discharges between doublets.

Figure 4.5 shows that increasing the discharge of a doublet causes larger spreading in the x-direction. This is not only caused by larger external ATES transport, but also by the larger area covered by the capture zones, which is a direct result of increasing the well discharge. When contaminant mass is transported to another doublet, it is mixed with the clean water within the extraction well and spread over the capture zone when injected again. In addition, when the contaminant can only be partly recovered afterwards, the spreading of the contaminant

by partial recovery has spread further. So the magnitude of the discharge also influences the spreading values.

Partial recovery by dispersion

Besides short circuit flow, there is another mechanism causing external ATEs transport. The dispersion at the boundaries of the injected water bodies causes partial recovery of the injected water. At the interface between two injecting wells, dispersion not only causes the contaminant to leave the capture zone of one well, but at the same time enters the capture zone of the same type of well in the opposite ATEs system. When the discharge regime changes, this contaminant mass is attracted and extracted by this same well in the opposite system. This results in an increase in contaminant concentration in the top right well in the second season (Figure 4.6).

Figure 4.6 shows the contaminant concentration in the top left well for different distances between the doublets (D_s). The distance between the opposite wells of the same ATEs systems is kept constant and is set to $1.85R_h$, which is large enough to eliminate the mass transfer through short circuit flow. If the short circuit flow was not eliminated effectively, the concentration in the top right well would already show an increase in the first season since there is always internal ATEs transport from the bottom right well towards the top right well. Figure 4.6 shows that the amount of external ATEs transport by dispersion depends on the distance between the two doublets. This makes sense, since a smaller distance between the doublets causes a larger interface area between the injected water volumes in the subsurface. When the area along which dispersion takes place increases, the amount of transport by dispersion will also increase.

When the distance between the doublets is $1.25R_h$ or smaller, the detected concentrations are higher than the threshold concentrations within the first year. This means that after the contaminant mass is mixed by dispersion, attracted towards the same well in the opposite ATEs system and mixed within that well, the contaminant is not diluted to concentrations below the threshold value. However, when the distance between the doublets is $1.5R_h$ or larger, the transport between the doublets is below the threshold value and thus negligible within the first year. Nevertheless, the partial recovery due to dispersion can cause external ATEs transfer at larger distances. Figure 4.6 shows for example that the doublets at a distance of $1.5R_h$ already show a more significant detected concentration after two years.

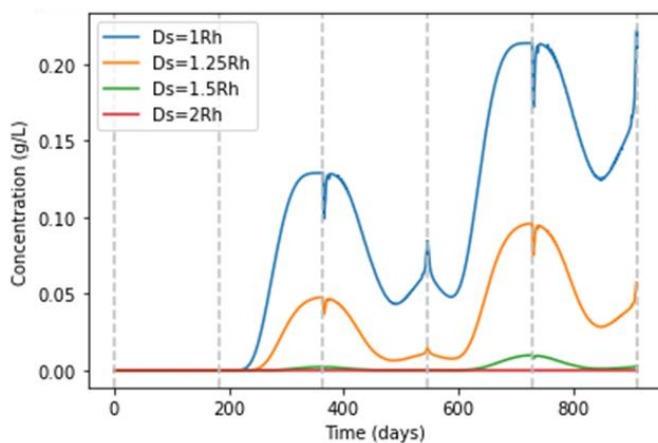


Figure 4.6 2x2 line pattern : The concentration in the top right well for different D_s values. $D_o = 2R_h$ ($3.25R_{th}$).

Besides the size of the area along which dispersion can take place, the magnitude of the dispersion is also important. Figure 4.7 shows the external ATEs transport by dispersion for different dispersivity values. As expected, the larger the dispersivity, the larger the amount of transported contaminant mass. The graph to the left shows that a doubling of the dispersivity results in a doubling of the concentrations found in the initially clean wells (within the first year). The approximately 8% of mass transfer in the first year when dispersivity equals 1.75 m, shows the significant contribution of dispersion on the whole contaminant plume. It should be noted that these rates of mass transfer are calculated for the high density scenario. For larger well distances, the influence of dispersion is expected to be smaller. The dispersivity value used in the model scenarios is 0.5 m, which is represented by the orange line. The blue line still shows an increased concentration while the dispersivity equals zero. This is caused by numerical dispersion.

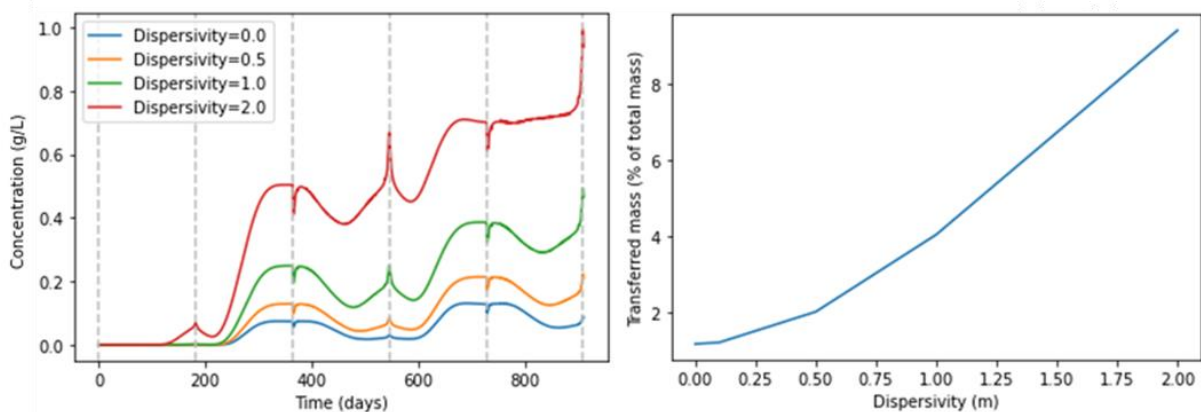


Figure 4.7 Left: Concentration in top right well for different dispersivity values. $D_s=1R_h$ ($1.63R_{th}$) and $D_o=2R_h$ ($3.25R_{th}$). Right: Amount of mass pumped by the top right well within the first year relative to the initial mass in the system.

4.1.3 High and low density scenario

The normalized results of the high and low density scenario are shown in Table 4.1. This table shows that the spreading and dilution in the x-direction is twice as large in the high density scenario compared to the low density scenario. Based on the observations in section 4.1.1 and section 4.1.2, this difference is caused by:

- Increased external ATEs transport by dispersion for smaller well distances.
- External ATEs transport by short circuit flow which only occurs in the high density scenario.

This also translates to the movement of the contaminant plume (Figure 4.8). In the high density scenario, the contaminant plume is initially pushed further to the left (away from the wells) due to the larger lateral spreading caused by the smaller distance between the doublets. However, the larger external ATEs transport rate causes the plume to move more towards the right over time. This transport even causes the spreading and dilution to become larger in the high density scenario, albeit the distance between the wells and thus the reach of the capture zones is smaller. In the low density scenario the contaminant plume keeps moving to the left over time, indicating that the spreading by partial recovery due to

dispersion plays a more important role in the spreading and dilution than the external ATES transport by dispersion.

	HDL	LDL
Center of mass (x,y)	(-0.44 , 0.87)	(-0.19 , 0.79)
Normalized variance x	23.1 (100%)	12.0 (52%)
Normalized variance y	24.6 (100%)	22.6 (92%)

Table 4.1 Normalized center of mass and variance results for the high density line (HDL) and low density line (LDL) scenario. The percentages are added to make it easier to compare the results.

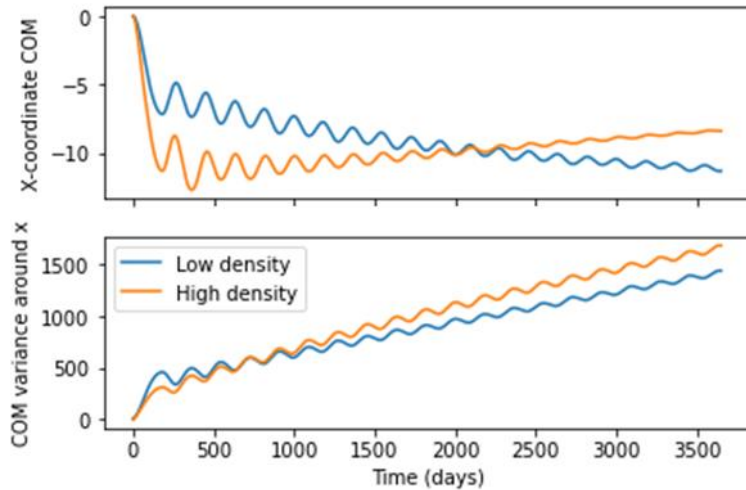


Figure 4.8 Center of mass (m) (top graph) and variance (m^2) (bottom graph) results over time for high and low density line pattern scenarios (HDL and LDL)

4.1.4 Conclusions

External ATES transport between two doublets in line pattern is governed by dispersion and short circuit flow, which depend on the well distances, dispersivity and relative well discharges between ATES systems:

- External ATES transport by short circuit flow only occurs in the high density scenario.
- External ATES transport by dispersion plays an important role and increases with decreasing distance between the doublets and also depends on the magnitude of dispersion. (For $D_s < 1.25R_h$, the concentrations in the right doublet exceed threshold concentrations).
- The high density scenario causes the spreading and dilution in the x-direction to double compared to the low density scenario.
- Differences in well discharge between ATES systems cause higher external ATES transport rates by increased short circuit flow and thus more spreading.

4.2 Interaction between two doublets in checkerboard pattern

4.2.1 Description observed plume development

The spreading of the contaminant by two checkerboard pattern doublets is visualized in Figure 4.9. In this figure, the internal and external ATEs transport by short circuit flow between opposite wells are visible. Due to the short circuit flow between the top left and top right well and the internal ATEs transport between the top right and bottom right well, the contaminant spreads over all four wells within one season. In this well configuration, there is also a sharp interface between the wells with the same temperature. However, this interface does not play a role in limiting mass transport between doublets as the location of the interface changes between seasons and the transport by short circuit flow is dominant.

The short circuit flow results in a contaminant plume which is located between the four wells. The contaminant plume moves towards the center as the short circuit flow, well dilution and internal ATEs transport cause the contaminant to be distributed over the wells and in the subsurface more evenly through time. The left graphs of Figure 4.10 show this movement towards the center of the four wells over time with the increasing x-coordinate value. The closer the doublets are, the further the contaminant plume moves towards the center. This indicates that the external ATEs transport increases with decreasing distance between the doublets. The right graphs in Figure 4.10 show that the closer the doublets are, the larger the spreading and dilution values in the x-direction. This is also caused by the increased external ATEs transport.

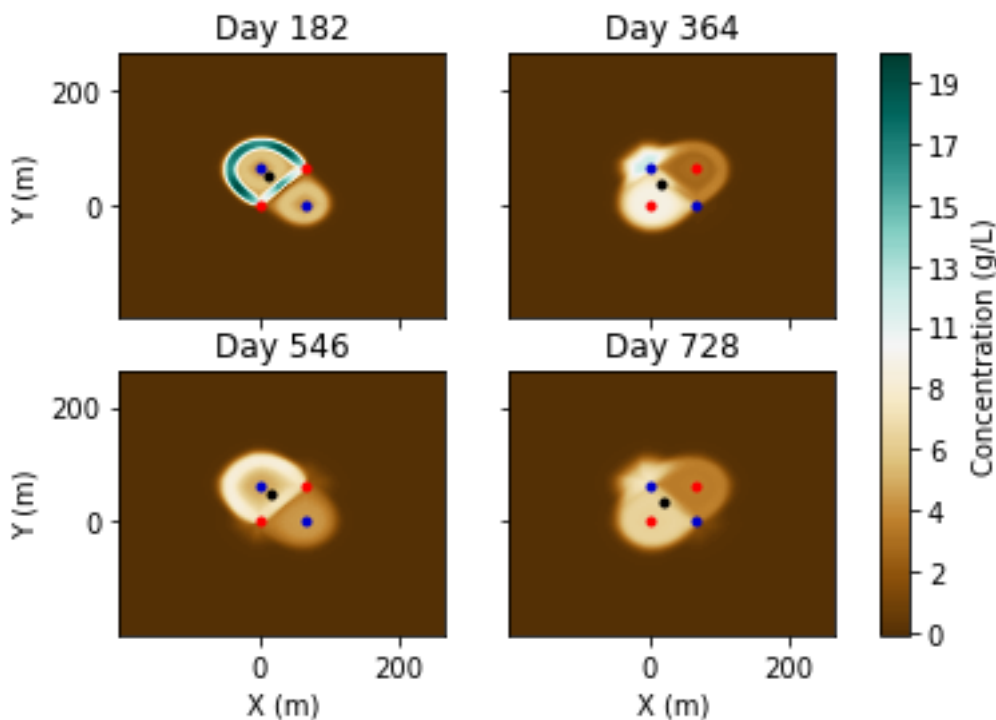


Figure 4.9 Contour plots of the contaminant distribution after 182, 364, 546 and 728 days. Generated by the high density checkerboard (HDC) scenario. The black dot marks the location of the center of mass.

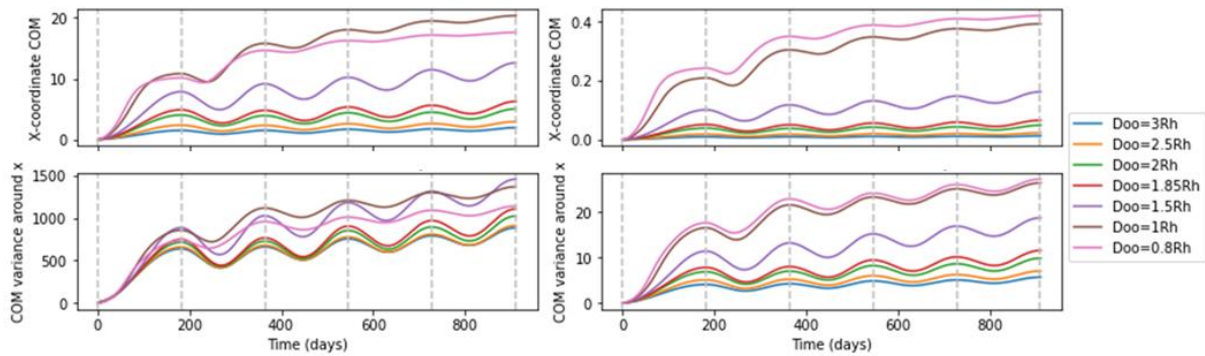


Figure 4.10 Left: Center of mass and variance results for different distances between the checkerboard doublets (D_{oo}). Right: Same results normalized for the well distances. $D_o = 1.85 R_h$.

4.2.2 External ATES transport in checkerboard pattern

Short circuit flow

Figure 4.11 shows the magnitude of the external ATES transport by short circuit flow between two checkerboard patterns for different distances between the doublets. The graphs show the concentrations detected in the top right well through time. Striking about this graph is that when the doublets are 1.5Rh and 1Rh apart, the concentrations are relatively high. In addition, the concentration decreases through time. The concentration is high because the distance is small enough for short circuit flow to occur and also for the largest part of the 'contaminant ring' to reach the other doublet. That is also why the concentration increases and decreases within the same season. The peaks in the graph become lower through time because these high concentrations are diluted by well dilution, dispersion and partial recovery. More and higher rates of interaction generally causes the overall concentration and therefore also the detected concentration to be lowered through time. The concentrations detected for $D_{oo} \geq 2R_h$ increase over time. Showing that a relatively small part of the contaminants reach the top right well within the first season and partial recovery will eventually cause more and more of the contaminant to move towards the capture zone of the right doublet. Since the wells of the two doublets have the same well discharge, the mass transfer by short circuit flow shown in Figure 4.11 is expected to be equal to the mass transport in the subsurface between the opposite wells of the same ATES system.

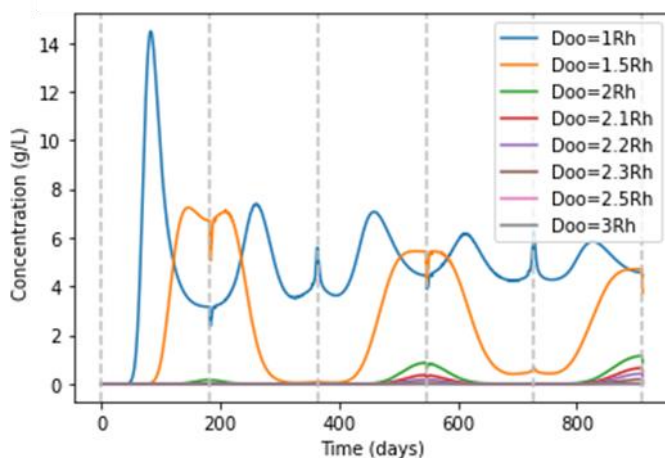


Figure 4.11 The concentration in the top right well for different distances D_{oo} .

To test at which distance the short circuit flow occurs, the dispersivity is set to zero and the distances between the two doublets is varied again. In Figure 4.12, the detected concentration in the top right well is shown for different D_{oo} values. This figure shows that short circuit flow occurs when D_{oo} is equal or smaller than $2.2R_h$. This distance is equal to $3.6R_{th}$, which is larger than the policy distance between two opposite wells.

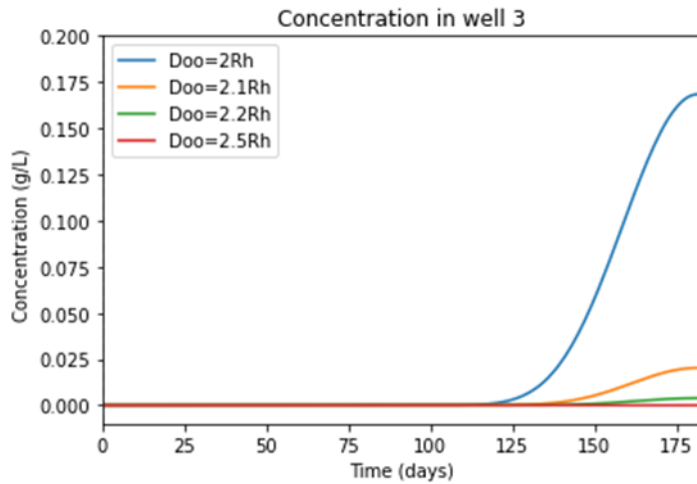


Figure 4.12 Contaminant concentration in top right well during the first season.

Figure 4.13 shows that including dispersion in the model causes the concentrations detected in the top right well to be higher and the short circuit flow to occur earlier. This effect becomes smaller through time. This figure shows, together with Figure 4.12, that the assumption that capture zones need to overlap for mass transfer to occur within one season (as described in section 2.4.5) is too simple and thus not true.

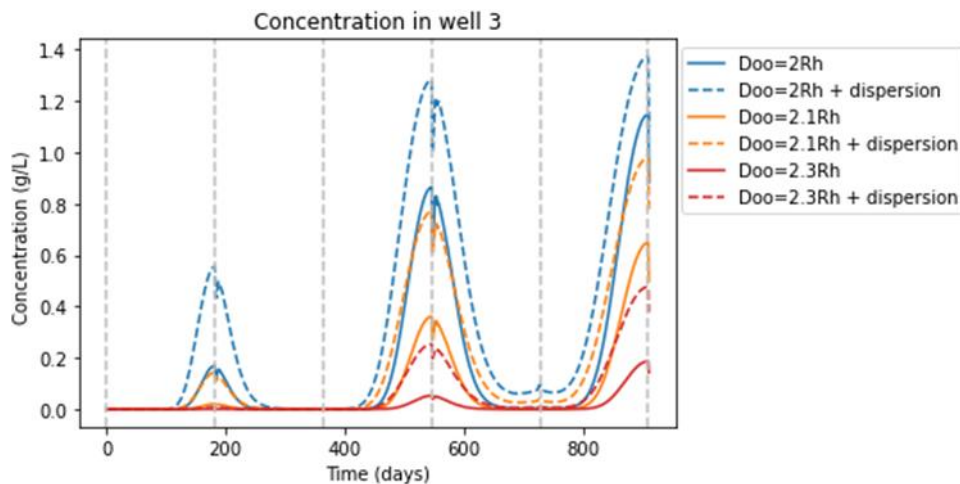


Figure 4.13 Contaminant concentration in the top left well for different distances between the doublets (D_{oo}) with and without dispersion.

4.2.3 High and low density scenario

In Table 4.2 the normalized results are shown for the low density scenario and the high density scenario. These results show that in the HDC scenario the spreading in the x-direction is 1.6 times higher and the spreading in the y-direction is 1.4 times higher compared to the

low density scenario. These larger values are caused by more external ATEs transport which increase the distribution over all wells by internal and external ATEs transport and well dilution. This is also visible in the movement of the contaminant plume, visualized in Figure 4.14. In the high density scenario, the contaminant plume is strongly drawn to the center of the wells and the fluctuating movement in the y-direction is minimized. This fluctuation is caused by the internal ATEs transport in the doublets and is minimized when the transported masses become equal.

	HDC	LDC
Center of mass (x,y)	0.32 , 0.70	0.11 , 0.88
Normalized variance x	27.3 (100%)	17.4 (64%)
Normalized variance y	27.6 (100%)	19.8 (72%)

Table 4.2 Center of mass and variance results normalized for the distance between the wells for high density and low density checkerboard scenarios (HDC and LDC).

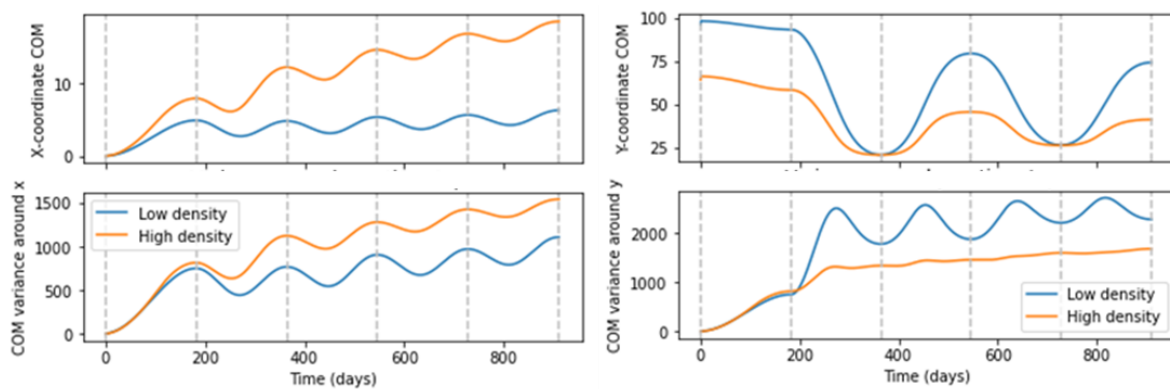


Figure 4.14 Center of mass (m) and variance (m^2) results in the x- and y-direction for high and low density checkerboard scenarios (HDC and LDC).

4.2.4 Conclusions

External ATEs transport between two doublets in checkerboard pattern is thus mainly governed by short circuit flow and partly influenced by dispersivity:

- Smaller distances between opposite wells of opposite ATEs systems (D_{oo}) cause larger external ATEs transport rates by short circuit flow. (Short circuit flow occurs when $D_{oo} \leq 2.2R_h$)
- Short circuit flow does not only occur when capture zones of opposite wells overlap.
- Dispersion influences the moment and magnitude of short circuit flow, but this effect diminishes over time and becomes smaller when the wells are closer together.

4.3 Comparison of line and checkerboard pattern

To conclude section 4.1 and section 4.2, Figure 4.15 shows the contour plots of all four scenarios after 2.5 years and Table 4.3 shows the corresponding average concentration, maximum concentration and normalized variance(x) after the 2.5 year runs. Both confirm that the checkerboard pattern causes most spreading and dilution because the external ATES transport is governed by short circuit flow, which is faster and causes more mass transfer than the transport by dispersion. This difference is mainly noticeable in low density scenarios, since short circuit flow also occurs in the high density line pattern. The external ATES transport between doublets is in general smaller when the distance between the wells is larger. The low density scenarios, based on the policy in the Netherlands, therefore show the lowest spreading and dilution values.

Scenario	Average concentration	Max. concentration	Variance(x) normalized
HDL	0.44	13.5	23.1
HDC	0.41	8.9	27.3
LDL	0.38	11.76	12.0
LDC	0.36	11.12	17.4

Table 4.3 The average concentration, maximum concentration and variance after the 2.5 year run.

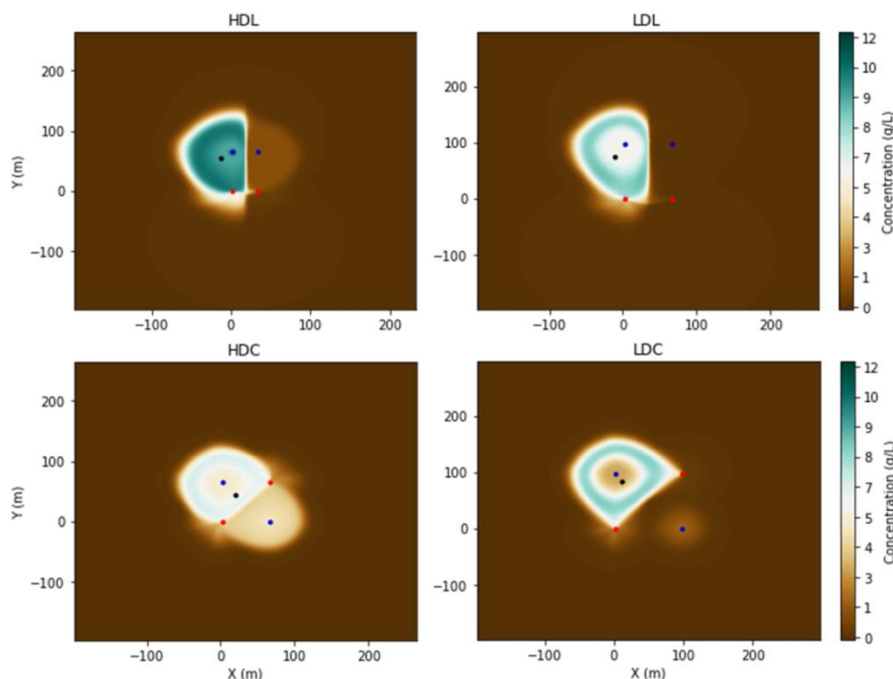


Figure 4.15 Contour plots of the four scenarios after 2.5 years.

4.4 Influence of ambient groundwater flow

4.4.1 Influence of ambient flow on the contaminant plume

To study the influence of ambient groundwater flow, a flow rate of 10 m/year was assigned to the four scenarios: high density line (HDL), low density line (LDL), high density checkerboard (HDC) and low density checkerboard (LDC). In Table 4.4, the changes in plume area, maximum concentration and average concentration are shown. These changes are expressed in percentages with the no flow scenarios as the reference scenario.

Scenario	Plume area	Maximum concentration	Average concentration	Variance x	Variance y
HDL	+ 6.49%	- 25.4%	- 6.11%	+63.0%	+4.7%
LDL	+ 4.45%	+ 16.9%	- 4.27%	+71.3%	+11.8%
HDC	+ 11.0%	+ 11.6%	- 9.91%	-4.5%	+1.9%
LDC	+ 6.17%	+ 20.1%	- 5.79%	+7.9%	+16.7%

Table 4.4 The percentage changes caused by adding ambient groundwater flow of 10m/year.

Table 4.4 shows that the plume area increases with the addition of ambient groundwater flow. This effect is best visible for checkerboard configurations and in high density scenarios. When the plume area is larger, the same amount of mass is spread over a larger area. Therefore, the average concentration becomes lower. The same was expected for the maximum concentration. However, the maximum concentration is only lower for the HDL scenario. In the other scenarios, the maximum concentration even increased. These larger maximum concentrations probably arise from groundwater volumes that are not or less often subject to well dilution.

As an example, the contour plot of the LDL scenario after 2.5 years is shown in Figure 4.16. This contour plot shows that the highest concentrations are present in the middle of the two doublets. This concentration probably remains high, because the ambient groundwater flow prevents part of the contaminated water to be extracted by the left doublet after injection. When the contaminated water is less often subject to well dilution, the maximum concentration will remain higher.

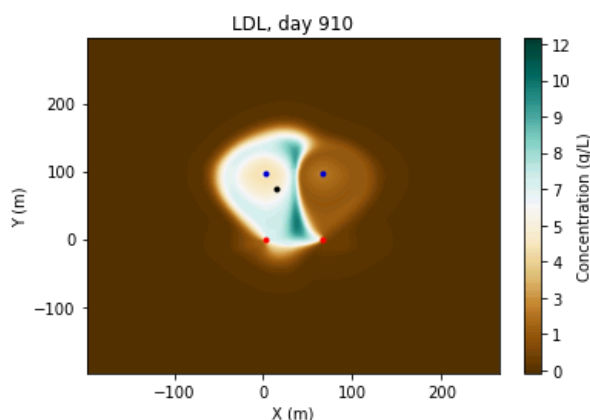


Figure 4.16 Contour plot low density line scenario (LDL) scenario with ambient groundwater flow.

Table 4.4 also shows an increase in spreading in both the x- and y-direction. This effect is best visible for the line pattern, since the external ATEs transport is increased significantly. The

ambient groundwater flow causes spreading by partial recovery and at the same time causes the contaminant to be transported into the capture zone of the right doublet. For checkerboard patterns, this external ATEs transport is already causing a large amount of spreading and dilution.

4.4.2 Influence of different flow velocities on the contaminant plume

To study the influence of different ambient flow rates on the contaminant plume, different flow velocities are applied to the high density checkerboard and line scenarios. Figure 4.17 shows the location of the contaminant plume after the 2.5 year runs. When only ambient groundwater flow influences the contaminant plume and the ATEs wells are turned off, the center of mass will move with the rate of the ambient groundwater flow. Meaning that for 1 m/year extra ambient groundwater flow, the x-coordinate of the plume will move 2.5 meters during the runtime. Figure 4.17 shows that for the line pattern, an ambient flow velocity of 1 m/year causes 2.4 meters movement of the plume. This is almost the same rate as in a system without wells.

However, in a system with a checkerboard pattern, the 1 m/year ambient groundwater flow causes the plume to move 1.8 meter. This is probably due to the lateral short circuit flow occurring between opposite wells of opposite ATEs systems in combination with internal ATEs transport. When contaminant mass is injected in the top left well, short circuit flow transfers part of the contaminant to the top right well. These contaminants are extracted by the top right well and injected in the bottom right well (internal ATEs transport). Short circuit flow then transports the contaminant from the bottom right to the bottom left well. This intensive interaction between the both doublets cause the contaminant mass to remain within the reach of the wells. These configurations thus actively transport the contaminant mass upstream. Therefore, the response is smaller. In case of the line pattern, only dispersion can cause upstream mass transport, which is considered negligible when compared to the partial recovery by the ambient flow.

The influence of the ambient groundwater flow on the contaminant plume location was also studied in the y-direction (Right graph in Figure 4.17). However, no conclusions can be drawn from those results since the outcome mainly depends on the activity of the wells right before the moment that is chosen to generate the results. The only conclusion that can be drawn is that the influence of the ambient flow is much smaller in the y-direction.

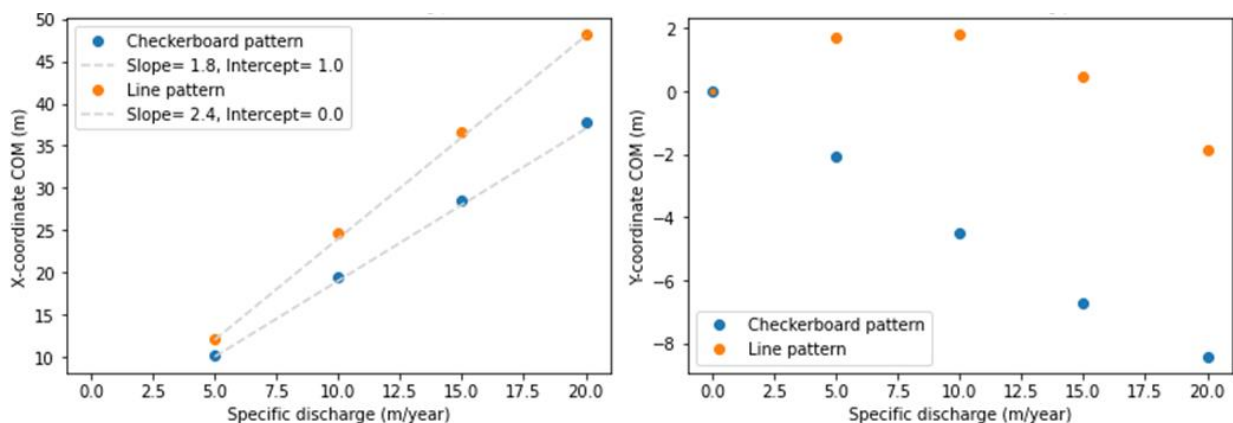


Figure 4.17 Influence of difference specific discharges on the location of the center of mass in the x- and y-direction.

Figure 4.18 shows the total variance (variance in x- and y-direction combined) for line and checkerboard patterns for different ambient flow velocities. This figure shows again that the checkerboard pattern is less sensitive to an increase in ambient flow compared to the line pattern.

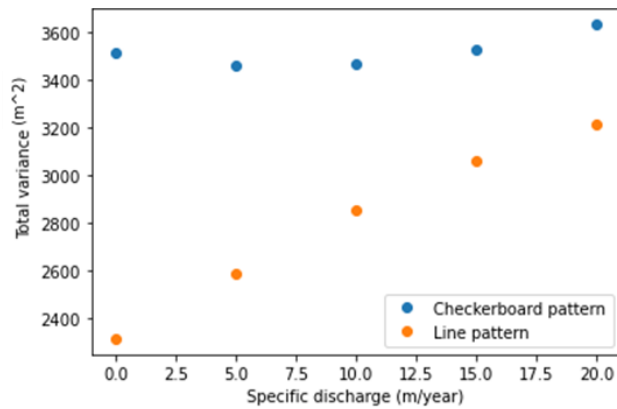


Figure 4.18 The total variance of the high density line (HDL) and high density checkerboard (HDC) scenarios after 2.5 years for different specific discharges.

4.4.3 Conclusions

Ambient groundwater flow causes increased spreading and dilution:

- Increased spreading and dilution is largest for checkerboard configurations and in high density scenarios.
- Ambient groundwater flow increases external ATEs transport and therefore increases the spreading and dilution (variance) results.
- The checkerboard pattern serves as an obstacle, slowing down the movement of the center of the plume.

4.5 Interaction between 4x4 ATES regions and contaminants

4.5.1 Spreading and dilution in line and checkerboard regions

To study the influence of an ATES region with a certain well density on the spreading and dilution of contaminants, eight doublets were placed in a high density and a low density scenario in line and checkerboard pattern. The resulting contaminant plumes after one season and after 10 years are shown in Figure 4.19. The same contour plots including ambient groundwater flow are shown in Figure 4.20.

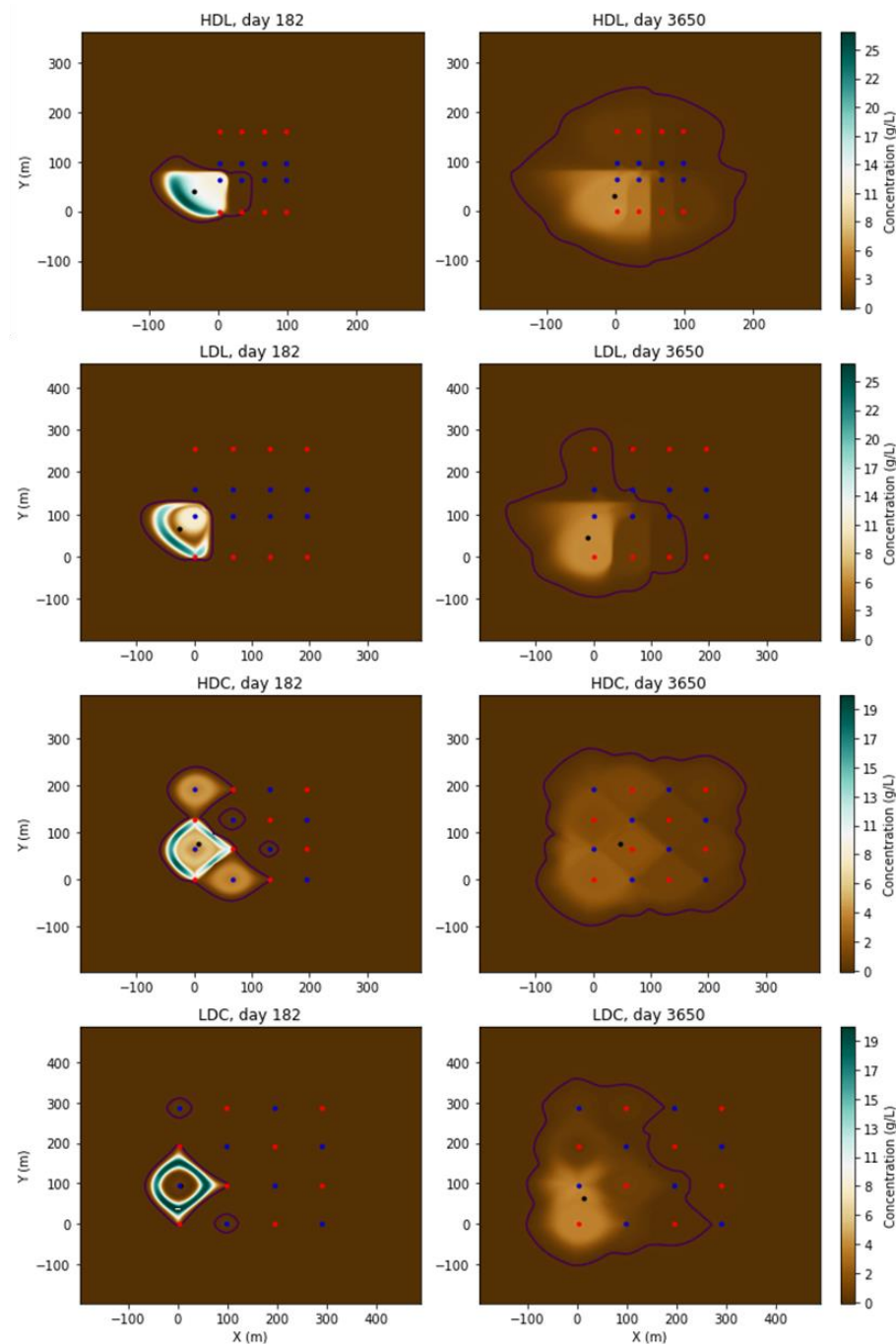


Figure 4.19 Eight contour plots which show the four 4x4 scenarios without ambient flow. The black dot marks the location of the center of mass and the purple line shows the average threshold concentration (0.014).

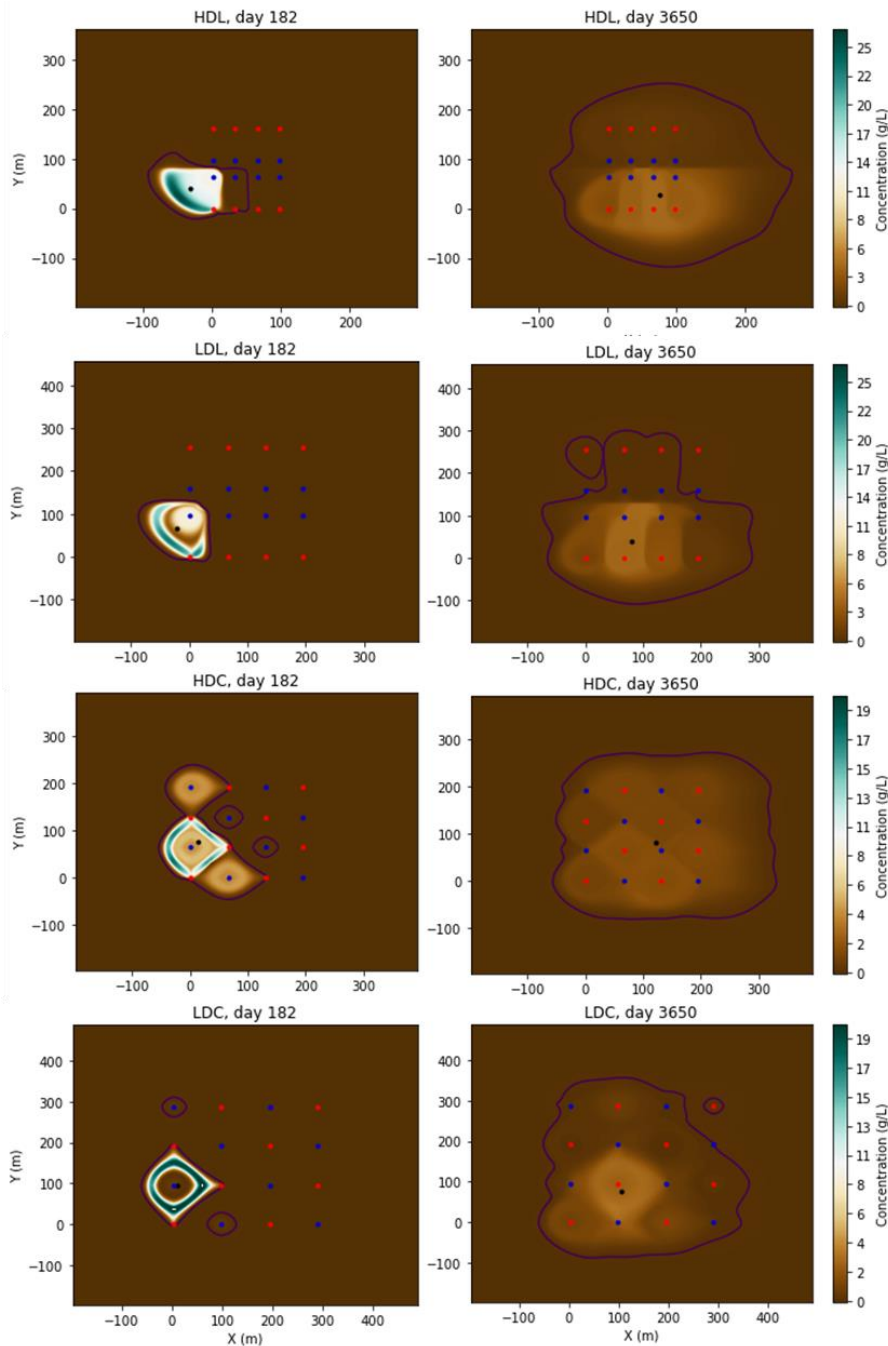


Figure 4.20 Eight contour plots which show the four 4x4 scenarios with ambient flow. The black dot marks the location of the center of mass and the purple line shows the average threshold concentration (0.014).

Movement contaminant plume

The studied external ATES transport plays a key role in the contaminant transport through high density ATES regions. As shown in section 4.1.3, the external ATES transport between two doublets is twice as large for the high density line (HDL) scenario compared to the low density line (LDL) scenario. As shown in Table 4.5 and Table 4.6, this is translated to both the movement of the contaminant plume, which is 2.4 times as large, and the spreading (variance), which is 2.2 times as large, in the high density pattern. The same goes for the checkerboard patterns. Section 4.2.3 shows that the high density scenario causes the variance

to become approximately 1.5 times larger in the x- and y-direction compared to the low density scenario. Table 4.5 and Table 4.6 show that the contaminant plume moves with a velocity which is 1.2 times larger than in the low density scenario. In addition, the spreading (variance) is 2.1 times larger in the high density scenario than in the low density scenario. The contaminant plume velocities increase when ambient flow is included in the scenarios (Table 4.6).

The differences in the velocity of the contaminant plume movement become smaller with the addition of ambient flow (Table 4.6). This applies to the difference between high and low density scenarios, but also to the difference between line and checkerboard patterns. This shows that the importance of the well patterns and well density decrease with increasing groundwater flow rate. The differences in contaminant spreading and the movement of the contaminant plume are also shown in the contour plots of Figure 4.19 and Figure 4.20.

Density	Pattern	Variance x-direction	Variance y-direction	Total variance
High	Line	23.6 (285%)	18.6 (174%)	42.2 (223%)
Low	Line	8.28 (100%)	10.67 (100%)	18.95 (100%)
High	Checkerboard	27.5 (332%)	33.6 (315%)	61.1 (322%)
Low	Checkerboard	8.77 (106%)	20.3 (190%)	29.07 (153%)

Table 4.5 The variance for all four scenarios with the low density line (LDL) scenario as a 100% scenario to compare the results.

Density	Pattern	Plume velocity (m/year)	Plume velocity (m/year) with ambient flow
High	Line	3.3	8.73
Low	Line	1.4	8.99
High	Checkerboard	4.1	11.38
Low	Checkerboard	3.4	10.89

Table 4.6 The velocities of the plume (center of mass) in the scenarios without and with ambient flow.

Table 4.6 shows that ambient flow is slowed down by the line pattern and is accelerated by the checkerboard pattern. However, in section 4.4.2, the checkerboard pattern was described as a 'blockage' to slow down contaminant transport. This difference can be explained by the scale and amount of wells. In this section, the movement of the contaminant plume through a field of ATES systems is studied. This movement is governed by the interaction between different ATES doublets and therefore high for checkerboard patterns and low for line patterns. In section 4.4.2 the influence of 2 checkerboard doublets within the flow path of the groundwater is studied. In that case the interaction between different ATES systems is counteracting the transport of contaminant downstream by ambient flow and thus slows down the movement of the contaminant plume.

Concentrations and extent of the contaminant plume

The maximum concentrations of checkerboard patterns are half the size of the maximum concentrations of the line patterns (without ambient flow) (Table 4.7). This shows that the larger contaminant spreading in checkerboard patterns indeed cause for the even spreading of the contaminant plume.

Density	Well pattern	Maximum concentration (no flow)	Maximum concentration (v=10 m/yr)
High	Line	6.2	4.2
Low	Line	7.5	4.0
High	Checkerboard	2.8	2.0
Low	Checkerboard	4.2	3.4

Table 4.7 The maximum concentrations after 10 years for the four scenarios with and without ambient flow.

Figure 4.21, shows the development of the plume area for the four scenarios. Since the 4x4 configurations are created to obtain results which can be extrapolated to larger ATES fields, it is important that the influence of the configuration boundaries is limited. All wells in the high density checkerboard configuration are contaminated, with concentrations higher than the threshold concentration, after 2.75 years. In the high density line (HDL) scenario, this occurred after 5.25 years. In the graphs of Figure 4.21, these moments mark a change in trend. The steep front represents the spreading and dilution of the contaminant plume through the ATES field. The second part of the graphs show the spreading by partial recovery outside the area in which the wells are located. This graph thus changes shape because the boundaries of the configuration are reached. This shows that the boundaries do influence the results. However, the relative plume area results are the same after 5 and 10 years (Figure 4.22). This shows that the boundaries of the model do not blur the differences in the results between scenarios, but that the time span over which the results are generated should be reconsidered. The differences in the results are achieved after 5 years already, so the actual differences in the results after 10 years are probably larger. The size of the well framework thus limits the amount of representative runtime.

Figure 4.20 and Figure 4.21 show that the plume area is much larger for the high density line pattern compared to the high density checkerboard pattern. Line patterns limit the amount of spreading and dilution by the smaller external ATES transport, but the increased hydraulic head differences caused by placing the same type of wells together still causes those relatively low concentrations to spread with the induced flow. This causes the high density line (HDL) scenario to produce a plume area which is a factor 5 larger compared to the low density (LDL) scenario (Figure 4.21).

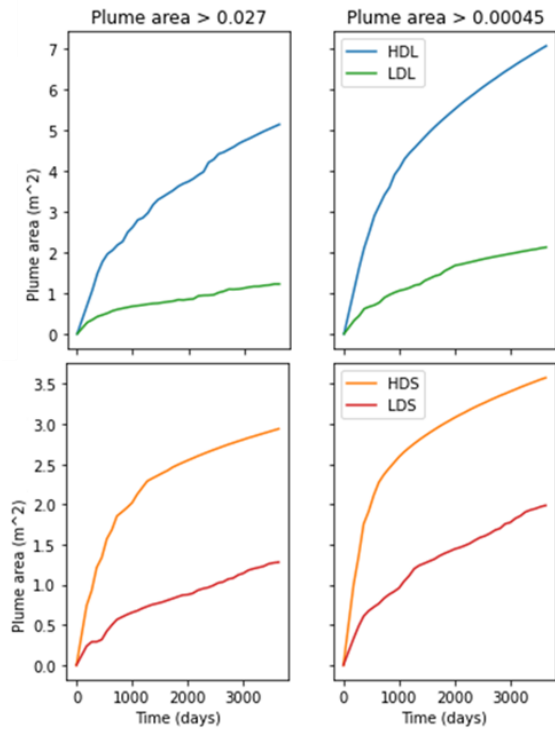


Figure 4.21 The top two graphs show the corrected plume area through time for the HDL and LDL scenarios for two intervention values. The bottom two graphs show the same, but for HDC and LDC.

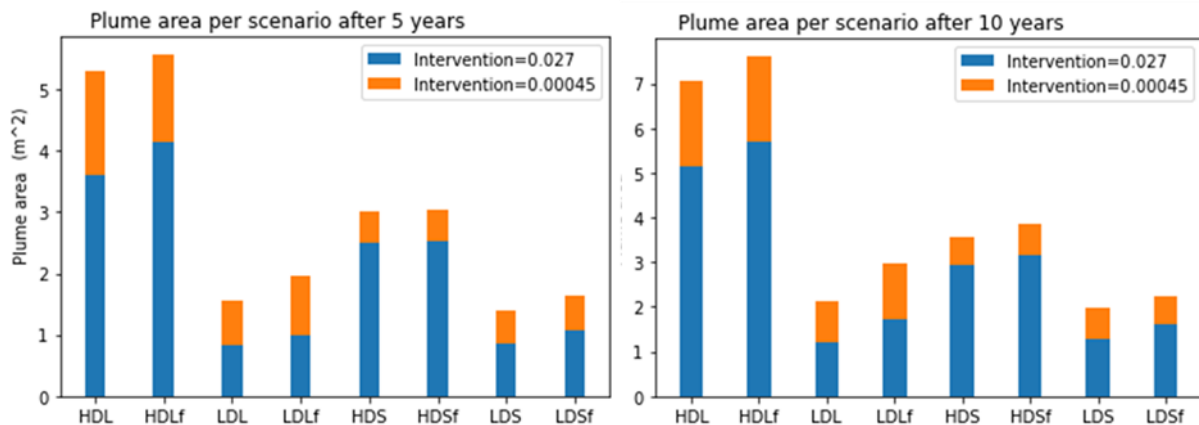


Figure 4.22 Relative plume area results after 5 and 10 years for two threshold concentrations.

Reference plume

To evaluate the impact of ATES systems on plume area, the plume area results were also compared to the reference plume development without ATES (Table 4.8). In the reference scenario, only dispersion causes the spreading of the contaminant and thus the plume growth. These plume area results are not normalized for the initial area of the well framework. At first, this table shows that the presence of ATES systems cause an enormous increase in the amount of spreading. Especially the checkerboard patterns show the creation of large plumes. The high density scenarios show the largest growth and the difference in scenarios of the line patterns is much larger than the difference in scenarios of the checkerboard patterns.

Scenario	Initial plume (day 41)	Plume area after 10 years	Factor growth
HDL	3268.0	78836	24.12
LDL	3356.0	60032	17.89
HDC	3476.0	108384	31.18
LDC	3500.0	106178	30.33
LDLref	3356.0	9068	2.7

Table 4.8 The plume areas for the four scenarios and the reference scenario which are calculated with an intervention value of 0.027.

4.5.2 Conclusions

The main conclusions of this section (4.5) are outlined below:

- The trends in the first 5 years can be extrapolated to larger ATES fields.
- Increasing ambient flow causes the influence of the well patterns to be of less importance.
- External ATES transport is a key mechanism in plume movement through a low, but especially high density ATES region.
- Implementation of ATES systems cause the spreading and dilution to increase very much.

5 Discussion

In this chapter, the results of this study are discussed and related to practice situations. In the first part, different spreading mechanisms are discussed, including consequences for ATES planning. The second part discusses the model used. This chapter is concluded with recommendations for further study.

5.1 Spreading and dilution by ATES systems

5.1.1 Spreading through ATES regions

The spreading and dilution through ATES systems in line pattern is dominated by external ATES transport by dispersion. This results in relatively low spreading rates. Furthermore, this spreading mechanism occurs at the timescale of one year. For the checkerboard pattern, the spreading and dilution is dominated by external ATES transport by short circuit flow, which causes large spreading rates and occurs at the timescale of one season. In practice, ATES systems are not placed in perfect line or checkerboard patterns, but the interaction between wells of the same type and wells of different type remain.

Preventing the increased spreading and dilution with the implementation of ATES systems is not realistic since spreading and dilution will inevitably increase. However, the large impact that the ATES systems have can be limited. This study showed that placing wells in line patterns limit the spreading and dilution most. Meaning that it is best to cluster wells of the same type in the subsurface. When wells of the same type are relatively close, the external ATES transport is restricted to dispersion. It is important to keep the wells of opposite type at a sufficient distance, since short circuit flow can still occur when the opposite wells are too close (as in the HDL scenario). When the policy distance of three times the thermal radius is applied between wells of opposite type, short circuit flow in line pattern is prevented. The clustering of the same type of wells and the sufficient distance between opposite type wells also benefit the thermal efficiency of the ATES systems.

5.1.2 Ambient flow

Ambient flow generally causes larger contaminant plumes and more spreading and dilution, since spreading by partial recovery and dispersion increase. This increased spreading is largest for the line pattern, because this spreading is normally limited by dispersion. When including ambient flow, the spreading by partial recovery increases significantly. The checkerboard pattern already causes large spreading and dilution rates to occur. Therefore, including ambient flow shows a less significant increase. This study shows that including ambient flow causes smaller differences in spreading and dilution in different configurations. Meaning that with larger ambient flow rates, the well configurations are less important. The differences that are still visible between the different configurations show that the line pattern is still the best option for limiting mass transfer as explained in section 5.1.1.

When only a few ATES wells are placed, checkerboard configurations can delay the transport of contaminant mass downstream as shown in section 4.4.2. However, in high density ATES regions, the plume moves relatively fast through the checkerboard pattern. When decreasing the well distances to use the subsurface more efficiently, the plume moves through the subsurface even faster.

5.1.3 Partial recovery by well imbalance

The seasonal imbalance between heating and cooling demand is not analyzed in this study. However, ATES systems are almost never in perfect balance. A severe winter could, for example, cause larger volumes of warm water to be pumped in a shorter amount of time, causing an imbalance in warm and cold water volumes. Also, a longer summer period in which cooling demand exist for longer than six months can cause imbalance. If these imbalances between the wells are known or can be predicted, these could be used in limiting the contaminant spreading. The wells with the largest discharge could be placed downstream. In that case, the downstream well causes less spreading due to partial recovery, because the period in which contaminated groundwater is injected and can be transported away from the well is relatively short. In addition, the contaminants that are not recovered by the upstream well which has a large injection period, are extracted by the well downstream. This approach would be especially suitable for a situation in which ambient groundwater flow rates are significant.

However, when considering the thermal efficiency of an ATES system, it is not favorable to place two different types of wells parallel to the groundwater flow. When ambient groundwater flow increases, the efficiency of the ATES system decreases especially in checkerboard patterns. To conclude, the above method could be useful in limiting contaminant spreading, but not for optimizing the thermal efficiency of the ATES systems.

5.1.4 Spreading and dilution by ATES systems with multiple wells

In this study, the spreading and dilution by doublets is studied. However, there are a lot of ATES systems which consists of more than two wells. This will cause the spreading and dilution by internal ATES transport to be much larger. Therefore, the contaminant concentrations will reduce relatively fast. In addition, the larger number of wells will cause the contaminant to spread in more locations and therefore at larger distances in the same time framework.

These larger systems could be of use in water treatment. When multiple wells belong to the same ATES system, the discharge volumes are all mixed within that system. The total amount of water in that system is therefore larger. When the water in this system is treated, only one treatment location is needed for a relatively large amount of water originating from a relatively large area in the subsurface.

5.1.5 Increased leaching from a constant contaminant source

As described in section 2.4.6, NAPLs are present in the subsurface in pure form and act as a constant contaminant source. From this constant source, contaminants dissolve into the groundwater that passes its location. The placement of ATES wells causes more groundwater flow and thus more leaching from those contaminant sources. This increased leaching is especially expected to occur in line pattern configurations, since the influence on the hydraulic heads is relatively large. Therefore, line pattern configurations might be unsuitable when pure NAPLs are present. In that case the larger plumes created by line patterns will also contain higher concentrations. On the other hand, the contaminated water from increased leaching is spread relatively fast through a checkerboard pattern. This rapid spreading and dilution will cause the concentrations to drop relatively fast, resulting in more contaminant mass that can dissolve in the groundwater.

In conclusion, it is important to know what kind of contaminants are present in the subsurface and in what form. If NAPLs are present, it is favorable to keep a sufficient distance between the ATES wells and the NAPLs. Further study is needed to gain insight in these required distances from contaminant sources. To study this, the vertical variation and vertical spreading should also be taken into account. When the vertical variation is included, the influence of properties like filter length can also be studied.

5.1.6 Management of contaminants

How contaminant spreading and dilution can be managed depends on the kind of contaminant source. Therefore this should be considered when choosing a management strategy. The two main types of contaminants present and their management strategy are outlined below:

- NAPLs: NAPLs form a constant contaminant source in the subsurface. Increased groundwater flow by well activity can cause increased leaching from these contaminant sources as explained in section 2.4.6. In this case, it is likely that the management goal is to limit spreading and dilution.
- Contaminant plume: When dissolved contaminants are present in the subsurface, the management strategy depends on the size of the contaminant plume and the proximity to groundwater protection zones. When for example, a contaminant plume moves towards a groundwater protection zone, it could be useful to dilute the plume to values below the intervention values. Preventing the contaminants to become a threat for drinking water production. When a large contaminant plume with high concentrations comes close to a groundwater protection zone, the strategy can still be to limit spreading and dilution to prevent health risks.

5.1.7 Implications for practice

In this section, some suggestions on ATES planning are stated which are based on the gained results:

- All ATES systems increase the spreading and dilution significantly. The LDL scenario causes the smallest plume area result (not normalized), but still causes the growth of the plume to be 6.6 times larger than the reference scenario after 10 years.
- Preventing mass transfer by external ATES transport is not realistic, since the distances at which this transport occurs are larger than the policy distance ($2.2R_h / 3.6R_{th}$ between opposite wells and $1.5R_h / 2.4R_{th}$ between the same type wells). Therefore, the location of the ATES wells should be based on the smallest mass transport between wells.
- The low density line patterns cause the contamination to travel through the well framework 2.4 times slower compared to the checkerboard pattern. For the high density patterns, the contamination only travels 1.2 times slower within line patterns, since short circuit flow occurs. The line pattern is thus most efficient in limiting contaminant spreading, especially when the opposite wells are at a sufficient distance.

- The checkerboard pattern can serve as a blockage for the transport of contaminants downstream if a small number of wells are placed in the flow path of a contaminant plume. This is caused by the external ATEs transport. In an ATEs region, this external ATEs transport causes the transport to be accelerated.
- The checkerboard patterns efficiently dilute contaminant mass. Mainly in the high density scenarios, the checkerboard patterns cause the maximum concentration to be twice as small as the maximum concentration in the line pattern. This goes for both with and without ambient flow.
- Internal ATEs transport causes a relatively fast way to move contaminants to another location. The checkerboard doublets in this study are placed perpendicular to the ambient groundwater flow. This is advisable, since the internal ATEs transport will cause even higher rates of plume movement through the high density ATEs regions
- In regions with large ATEs demands, the distance between wells can deviate from the policy distances in order to use the subsurface more efficiently. When the wells are placed closer together, especially the line pattern causes the plume area to increase. The relative spreading increases with a factor 5. This illustrates the influence on the hydraulic head.

5.2 Discussion on the used model

5.2.1 Internal ATEs transport

Section 3.3.4 explains how the internal ATEs transport is modeled in this study. This method performed well in this study and is, besides for doublets, also applicable for ATEs systems with multiple warm and cold wells. Four aspects should be noted when one uses this method:

- Mass extracted in the first time step is lost in the system since no water is injected in that first period.
- When the well discharge is zero in between seasons, the contaminant mass extracted in one time step earlier is temporarily saved during one season and then injected in the correct well.
- The sine discharge distribution causes the mass budget to fluctuate through time.
- The extracted mass is calculated with the final concentration after one time step, not including concentration changes within that time step.

These deviations from the practice application are not noticeable in the results of this study, because a small time step of 1 day was chosen. Another approach could be to run all time steps twice. In that case, the concentration results from the first calculation can be used as input for the second calculation to model the simultaneous extraction and injection of contaminant mass. Since the model worked excellent, this double calculation was not included in this study.

5.2.2 Influence of initial contaminant

In all scenarios, the contaminant is introduced in the bottom left doublet. As explained in section 3.2.3, this initial contamination was injected in one of the wells to be able to study the influence of the ATES wells on contaminated groundwater and to study what happens with the contaminated groundwater once it enters the capture zone of an ATES well. This enabled studying the spreading and dilution through the well framework with the location of the contaminant plume. Figure 5.1 shows the contour plots of a scenario in which the initial contamination is injected in another well. This causes the external ATES transport to also occur towards the left. Therefore, the plume location is relatively stable and stays at the same doublet while part of the contaminated groundwater spreads through the ATES region. In this alternative situation, the location of the contaminant plume would thus not give a lot of insight in the spreading and dilution. However, this situation does emphasize the limited spreading effect by maintaining a maximum concentration of 7.5 g/L instead of 6.05 g/L. It is important to note that in practice, this spreading occurs in all directions if ATES systems are nearby. The slight deviation of the contaminant plume towards the left (in the alternative scenario) is caused by the left model boundary which is slightly closer and therefore causes a steeper gradient.

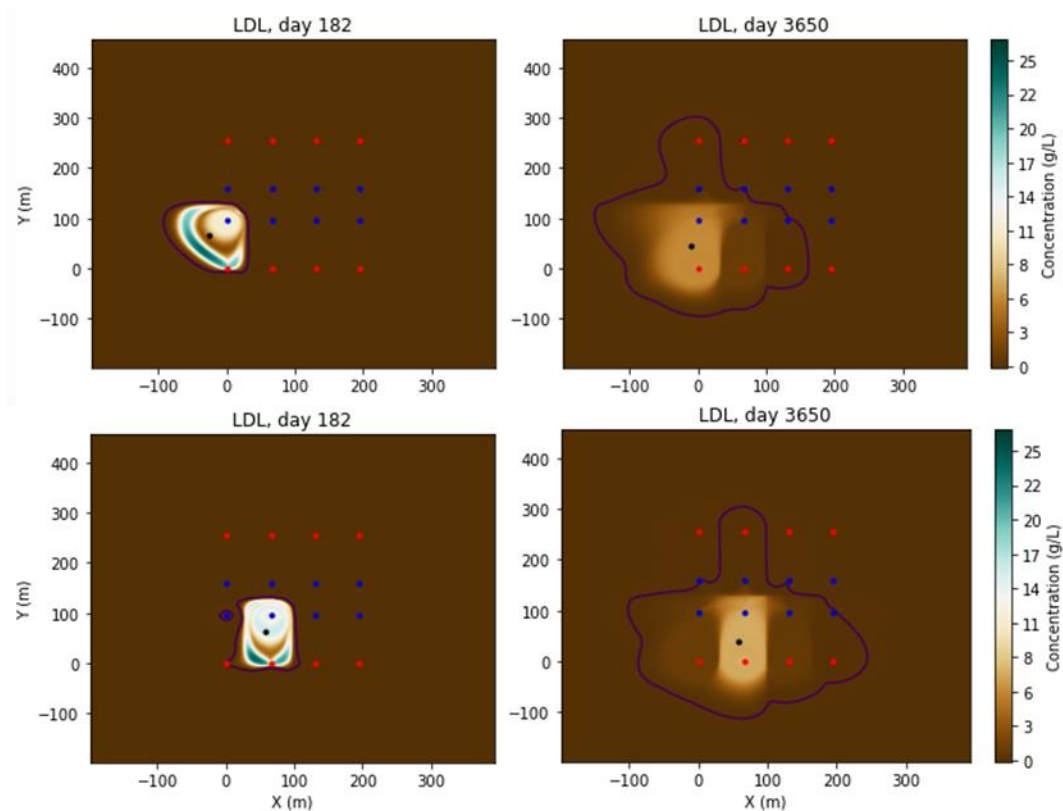


Figure 5.1 Four contour plots showing the influence of a different initial contaminant location.

5.2.3 Extrapolation of 4x4 configurations to larger regions

The 4x4 configurations are used to obtain spreading and dilution results which can be interpolated to larger fields of ATES systems. Hence the comparison of the results in this study based on the well density. As described in section 4.5.1, it is important to consider which run times will give representative results that are not influenced by the boundaries of

the configuration. Another way to obtain results based on the well density (in future research) is to choose a fixed area and fill that area with wells with a certain distance from each other.

5.3 Recommendations

In this section, some recommendations are done for further study:

- Further study needs to be done to learn more on the influence of adsorption on the contaminant plume. For highly adsorptive contaminants, the contaminated water front is expected to be retarded. Similar to the thermal radius, which is smaller than the hydraulic radius, the front of the contaminated water is also expected to extend less. Therefore, the adsorption is expected to slow down the growth and the travel time of the plumes. This could for example result in wells that can be placed closer together. Or in wells placed at policy distance between which no contaminant transport occurs within the first year.
- The model is created based on the situation in the city center of Utrecht. The ATES systems that are active in Utrecht are not placed in perfect line or checkerboard patterns. Therefore, a case study on Utrecht will give insight in the spreading and dilution in a more realistic and somewhat random well configuration. The results of this study can then be compared with the results of the case study.
- It is not always possible to find an optimal situation in which the thermal performance of the ATES systems is optimal, the spreading of contaminants can be minimized, the groundwater protection zones can be protected and the wells can be placed exactly at the desired locations. That is why other measures like pump and treat should also be explored. This can for example be done by using the short circuit flow between opposite wells to pump and treat a large amount of contaminated water.
- The contaminant transport in a high density ATES area with larger ATES systems should be investigated. Since larger ATES systems are expected to cause larger spreading and dilution rates.
- The variation in the vertical should be taken into account in future research. This enables studying increased leaching from constant contaminant sources. The distance between the wells and the contaminant source are expected to influence the amount of leaching. In addition, the filter length could be varied as an attempt to minimize the leaching.

6 Conclusion

In this thesis, the contaminant transport through ATES regions and the effects of well patterns and ambient flow on this transport are studied. This is done by implementing an internal ATES transport method, describing the contaminant plume development in different scenarios and by quantifying this spreading and dilution.

The 2x2 well configurations show that external ATES transport depends on well distances, dispersivity and relative well discharges between ATES systems. In general, the closer the wells are, the larger the spreading by external ATES transport. In line pattern, this transport is dominated by dispersion which causes low spreading rates at a timescale of a year. In checkerboard pattern, the external ATES transport by short circuit flow causes large spreading rates and occurs at the timescale of one season. The distances needed to prevent external ATES transport in both scenarios are larger than the policy distances and therefore too large to apply. The 4x4 configurations show that this external ATES transport translates to spreading rates through ATES regions and it is therefore a key factor in spreading and dilution. In practice, it would therefore be best if the wells of the same type are clustered in order to limit the amount of contaminant spreading. As long as the opposite wells are placed at a distance which prevents short circuit flow, this advantage will hold. This is also beneficial for optimizing the thermal efficiency of the ATES systems. When ambient flow rates increase, the different effects of well configurations become less pronounced and thus less important. However, the differences that can be observed show that the line pattern remains most suitable for limiting contaminant spreading. This is again positive for the thermal efficiency as the line pattern is from a thermal perspective most suitable when ambient flow rates are high.

In checkerboard patterns, the contaminant spreads more evenly through the well framework. This causes the velocity of the contaminant plume to be larger in this configuration. However, the line pattern scenarios cause much larger relative spreading rates. The concentrations in the resulting contaminant plume are much lower compared to the checkerboard pattern, since most mass remains concentrated around the center of the plume. Nevertheless, the extent of the plume is larger. This is caused by the large hydraulic head differences when wells of the same type are placed close together. This is important to consider in ATES planning, since this increased flow could cause larger spreading rates by increased leaching of constant contaminant sources. Additional study is needed to investigate this effect.

This study also shows that the short circuit flow in checkerboard pattern causes the transport of contaminants downstream of the wells to slow down when a small number of wells are placed in the flow path of a contaminant plume. This external ATES transport by short circuit flow does not only occur when capture zones overlap. The activity of the wells and dispersion cause mass transport to occur at distances which are slightly larger than two times the hydraulic radius.

This study quantified the spreading and dilution of contaminants in ATES regions and supported these results with studying external ATES transport between doublets. It showed that the activity of ATES wells always increases the amount of spreading and dilution, but also that limiting contaminant spreading and optimizing thermal efficiency can be combined. Further study should focus on expanding this knowledge on constant contaminant sources and the implementation of this knowledge in ATES planning.

References

- Bear, J.; Jacobs, M. (1965). *On the movement of water bodies injected into aquifers*. *Journal of Hydrology* Vol. 3, p. 37-57.
- Bloemendal, Martin. "The hidden side of cities: Methods for governance, planning and design for optimal use of subsurface space with ATEs." (2018).
- Bloemendal, M. and Hartog, N. (2018). *Analysis of the impact of storage conditions on the thermal recovery efficiency of low-temperature ATEs systems*. *Geothermics*, 71(October 2017):306–319.
- Bloemendal, M., Olsthoorn, T., & van de Ven, F. (2015). *Combining climatic and geo-hydrological preconditions as a method to determine world potential for aquifer thermal energy storage*. *Science of the Total Environment*, 538, 621-633.
- Bloemendal, M., Olsthoorn, T., & Boons, F. (2014). *How to achieve optimal and sustainable use of the subsurface for Aquifer Thermal Energy Storage*. *Energy Policy*, 66, 104-114.
- Bonte, M. (2013). *Impacts of shallow geothermal energy on groundwater quality. A hydrochemical and geomicrobial study of the effects of ground source heat pumps and aquifer thermal energy storage*. PhD thesis, Vrije Universiteit Amsterdam, Amsterdam, the Netherlands.
- Calje, R.J. (2010). *Future use of Aquifer Thermal Energy Storage below the historic centre of Amsterdam*. MSc thesis, Technische Universiteit Delft, Delft, the Netherlands.
- Deltares (2009). Borren, W.; Berendrecht, W.; Heijkers, J.; Snepvangers, J.; Veldhuizen, A. *Ontwikkeling HDSR hydrologisch modelinstrumentarium – HYDROMEDAH. Deelrapport 1: Beschrijving MODFLOW model*.
- Duijff, R. (2019). *Interaction between multiple ATEs systems: Analysis of thermal and geohydrologic performance*.
- Gelhar, L. W., Welty, C., & Rehfeldt, K. R. (1992). *A critical review of data on field-scale dispersion in aquifers*. *Water resources research*, 28(7), 1955-1974.
- Hartog, N.; Drijver, B.; Dinkla, I.; Bonte, M. (2013). *Field assessment of the impacts of Aquifer Thermal Energy Storage (ATEs) systems on chemical and microbial groundwater composition*. *European Geothermal Congress 2013*.
- Jaxa-Rozen, M., Kwakkel, J., & Bloemendal, M. (2015, August). *The adoption and diffusion of common-pool resource-dependent technologies: The case of aquifer Thermal Energy Storage systems*. In *2015 Portland International Conference on Management of Engineering and Technology (PICMET)* (pp. 2390-2408). IEEE.
- Kueper, B.H. and E.O. Frind (1991), *Two phase flow in heterogeneous porous media: 2. Model application*, *Water Resour, Res.*, 27, 1059-1070.
- Langevin, C. D., Thorne, D. T., Dausman, A. M., Sukop, M. C., and Guo, W. (2008). Chapter A22. In *SEAWAT Version 4: A Computer Program for Simulation of Multi-Species Solute and Heat Transport: U.S. Geological Survey Techniques and Methods Book 6*, page 39. USGS.
- Li, Q. (2014). *Optimal use of the subsurface for ATEs systems in busy areas. Towards more robust master plans using a two-stage assessment method*. MSc Thesis, Technische Universiteit Delft, Delft, the Netherlands.

Meer Met Bodemenergie rapport 3/4. Bioclear, Deltares, IF Technology and Wageningen Universiteit (2012). Effecten op de ondergrond. Effecten van bodemenergiesystemen op de geochemie en biologie in de praktijk. Resultaat metingen op pilotlocaties en labtesten.

Meer met Bodemenergie rapport 9. Bioclear, Deltares, IF Technology and Wageningen Universiteit (2012). Effecten op sanering. Effecten van bodemenergiesystemen bij inzet bodemsanering - resultaat metingen op pilotlocaties en in labtesten

Phernambucq, I. (2015). Contaminant spreading in areas with a high density of Seasonal Aquifer Thermal Energy Storage (SATES) systems. Msc, University of Utrecht.

REN21 (2017). Renewables 2017: Global Status Report. Technical Report October 2016, REN21.

*Sommer, W. T., Doornenbal, P. J., Drijver, B. C., van Gaans, P. F. M., Leusbrock, I., Grotenhuis, J. T. C., and Rijnaarts, H. H. M. (2014). Thermal performance and heat transport in aquifer thermal energy storage. *Hydrogeology Journal*, 22(1):263–279.*

Tauw bv (2010). Bloemendal, M.; Boerefijn, M.; Blonk, A.; Hoekstra, J.; Winters, G. M.e.r. Koude-Warmteopslag Stationsgebied Utrecht.

Zheng, C. (2010). MT3DMSv.5 Supplemental User's Guide

*Zuurbier, K.G.; Hartog, N.; Valstar, J.; Post, V.E.A.; Van Breukelen, B.M. (2013). The impact of low-temperature seasonal aquifer thermal energy storage (SATES) systems on chlorinated solvent contaminated groundwater: Modeling of spreading and degradation. *Journal of Contaminant Hydrology*. Vol. 147 p. 1-13. doi: 10.1016/j.jconhyd.2013.01.002*

List of symbols and units

Symbol	Description	Unit
R_h	Hydraulic radius	m
V_{season}	Volume injected in an ATEs well in one season	m^3
H	Filter length of the well	m
θ	Porosity	-
\bar{t}	Parameter to indicate the shape and deformation of a capture zone	-
D	Aquifer thickness	m
q	Specific discharge / ambient flow	m/day
t_q	Duration of injection or extraction	Days
Q	Well discharge	m^3/day
R_{th}	Thermal radius	M
c_w	Heat capacity of water	$\text{J}/\text{m}^3/\text{K}$
c_{aq}	Saturated heat capacity of the aquifer	$\text{J}/\text{m}^3/\text{K}$
x	Ratio between R_h and R_{th}	-
K	Hydraulic conductivity	m/day
h	Hydraulic head	M
S_s	Specific storativity	1/m
t	Time	Days
W	Sources and sinks	-
R	Retardation factor	-
C	Concentration of the solute	kg/m^3
ρ_b	Bulk density	kg/m^3
K_d	Distribution coefficient	m^3/kg
D_{tot}	Dispersion coefficient	m^2/day
q_s	Volumetric flow rate per unit volume of aquifer representing fluid sources or sinks.	1/day
C_s	Concentration of the fluid source or sink	kg/m^3
R_T	Thermal retardation	-
T	Temperature	K
$D_{T\text{tot}}$	Thermal dispersion coefficient	m^2/day
ρ_f	Fluid density	kg/m^3
μ_0	Dynamic viscosity at a reference concentration and temperature	$\text{kg}/(\text{m}/\text{day})$
μ	Dynamic viscosity	$\text{kg}/(\text{m}/\text{day})$
K_0	Hydraulic conductivity of the material when saturated	m/day
h_0	Hydraulic head measured at a reference concentration and temperature	M
ρ_0	Fluid density at the reference temperature and concentration	kg/m^3
z	Elevation head	M
K_v	Vertical hydraulic conductivity	m/day
α	Dispersivity	M
ρ_s	Density of solids	kg/m^3

List of figures

Figure 2.1 The working of an ATES system in The Netherlands (Bloemendal, 2018).....	6
Figure 2.2 The difference between the hydraulic radius Rh and the smaller thermal radius Rth . The length of the cylinder is determined by the filter length of the well (Duijf, 2019).....	8
Figure 2.3 The two most common well patterns: checkerboard pattern and line pattern.....	8
Figure 2.4 Well dilution, causing homogenising of natural vertical gradients and dilution of contaminants (Phernambucq, 2015).	9
Figure 2.5 Mixing by dispersion at the boundary of the injected water volume (Phernambucq, 2015).10	
Figure 2.6 Spreading and dilution by internal ATES transport. A: Internal ATES transport in a doublet; B: Internal ATES transport in a system with multiple wells (Phernambucq, 2015).	10
Figure 2.7 Partial recovery by ambient groundwater flow (Phernambucq, 2015).....	11
Figure 2.8 Connected capture zones which can cause transfer of contaminant mass between different ATES systems (Phernambucq, 2015).....	12
Figure 3.1 The sine discharge distribution of the warm and cold wells in the model.	16
Figure 3.2 The center of mass results for different grid sizes to determine the spatial resolution.	17
Figure 3.3 The center of mass results for different grid sizes to determine the temporal resolution. ..	17
Figure 3.4 The grid structure and parameters used in this study.	18
Figure 3.5 The 2x2 line configuration showing the definition of the distance between the wells with the same temperature (D_s) and the distance between the wells with the opposite temperature (D_o). The red wells are warm and the blue wells are cold. The yellow circle marks the well in which the initial contamination is injected.	20
Figure 3.6 The 2x2 checkerboard configuration showing the definition of the distance between two wells with opposite temperature within the same doublet (D_o) and the distance between the wells with opposite temperature and opposite doublet (D_{oo}). The red wells are warm and the blue wells are cold. The yellow circle marks the well in which the initial contamination is injected.	21
Figure 3.7 The direction of the ambient groundwater flow with respect to the wells.	22
Figure 3.8 The low density 4x4 line well configuration (LDL). The yellow circle marks the well in which the initial concentration is injected. The well framework consists of 8 ATES systems / 8 doublets. How these systems are aligned is shown with the grey boxes.....	22
Figure 3.9 The low density 4x4 checkerboard well configuration (LDC). The yellow circle marks the well in which the initial concentration is injected. The well framework consists of 8 ATES systems / 8 doublets. How these systems are aligned is shown with the grey boxes.....	23
Figure 4.1 Contour plots of the contaminant distribution after 182, 364, 546 and 728 days. Generated with the 2x2 high density line (HDL) scenario. The black dot marks the location of the center of mass.	26
Figure 4.2 Left: the location of the center of mass and the variance in the x-direction. Right: The same results normalized for the changing well distances.	27
Figure 4.3 Contaminant concentrations measured in the bottom right well during the first season for different distances between the wells (D_s and D_o).	27
Figure 4.4 The concentration in the bottom right well for different doublet discharges. The blue line represents the mass transfer for the high density line (HDL) scenario with equal discharges.	28
Figure 4.5 Variance (x) results for differences in well discharges between doublets.	28
Figure 4.6 2x2 line pattern : The concentration in the top right well for different D_s values. $D_o=2Rh$ ($3.25Rth$).	29
Figure 4.7 Left: Concentration in top right well for different dispersivity values. $D_s=1Rh$ ($1.63Rth$) and $D_o=2Rh$ ($3.25Rth$). Right: Amount of mass pumped by the top right well within the first year relative to the initial mass in the system.....	30
Figure 4.8 Center of mass (top graph) and variance (bottom graph) results over time for high and low density line pattern scenarios (HDL and LDL)	31

Figure 4.9 Contour plots of the contaminant distribution after 182, 364, 546 and 728 days. Generated by the high density checkerboard (HDC) scenario. The black dot marks the location of the center of mass.....	32
Figure 4.10 Left: Center of mass and variance results for different distances between the checkerboard doublets (Doo). Right: Same results normalized for the well distances.....	33
Figure 4.11 The concentration in the top right well for different distances Doo.....	33
Figure 4.12 Contaminant concentration in top right well during the first season.	34
Figure 4.13 Contaminant concentration in the top left well for different distances between the doublets (Doo) with and without dispersion.	34
Figure 4.14 Center of mass and variance results in the x- and y-direction for high and low density checkerboard scenarios (HDC and LDC).....	35
Figure 4.15 Contour plots of the four scenarios after 2.5 years.	36
Figure 4.16 Contour plot low density line scenario (LDL) scenario with ambient groundwater flow. ...	37
Figure 4.17 Influence of difference specific discharges on the location of the center of mass in the x- and y-direction.....	38
Figure 4.18 The total variance of the high density line (HDL) and high density checkerboard (HDC) scenarios after 2.5 years for different specific discharges.....	39
Figure 4.19 Eight contour plots which show the four 4x4 scenarios without ambient flow. The black dot marks the location of the center of mass and the purple line shows the average threshold concentration (0.014).	40
Figure 4.20 Eight contour plots which show the four 4x4 scenarios with ambient flow. The black dot marks the location of the center of mass and the purple line shows the average threshold concentration (0.014).	41
Figure 4.21 The top two graphs show the corrected plume area through time for the HDL and LDL scenarios for two intervention values. The bottom two graphs show the same, but for HDC and LDC.	44
Figure 4.22 Relative plume area results after 5 and 10 years for two threshold concentrations.....	44
Figure 5.1 Four contour plots showing the influence of a different initial contaminant location.....	50

List of tables

Table 3.1 Hydrogeological and transport parameters (MMB9, 2012 ; Tauw, 2010 ; Deltares, 2009)....	15
Table 3.2 Species specific used parameters.	15
Table 3.3 Model specifics based on information from MMB9 (2012), Tauw (2010) and Deltares (2009) for the two different model versions.	16
Table 3.4 The parameters determining the discretization and extent of the model as defined in Figure 3.4.	17
Table 3.5 The definition and distances between the wells for the four main scenarios.	20
Table 3.6 Solubility and intervention values for different contaminants and the factor used to calculate the threshold concentration in the model.	24
Table 4.1 Normalized center of mass and variance results for the high density line (HDL) and low density line (LDL) scenario. The percentages are added to make it easier to compare the results.	31
Table 4.2 Center of mass and variance results normalized for the distance between the wells for high density and low density checkerboard scenarios (HDC and LDC).	35
Table 4.3 The average concentration, maximum concentration and variance after the 2.5 year run. ...	36
Table 4.4 The percentage changes caused by adding ambient groundwater flow of 10m/year.	37
Table 4.5 The variance for all four scenarios with the low density line (LDL) scenario as a 100% scenario to compare the results.	42
Table 4.6 The velocities of the plume (center of mass) in the scenarios without and with ambient flow.	42
Table 4.7 The maximum concentrations after 10 years for the four scenarios with and without ambient flow.	43
Table 4.8 The plume areas for the four scenarios and the reference scenario which are calculated with an intervention value of 0.027.	45